

[Fe₁₅]: A Frustrated, Centred Tetrakis Hexahedron

Daniel J. Cutler,^a Mukesh K. Singh,^a Gary S. Nichol,^a Marco Evangelisti,^b Jürgen Schnack,^{*c} Leroy Cronin^{*d} and Euan K. Brechin^{*a}

^aEaStCHEM School of Chemistry, The University of Edinburgh, David Brewster Road, Edinburgh, EH9 3FJ, Scotland, UK. E-mail: ebrechin@ed.ac.uk.

^bInstituto de Nanociencia y Materiales de Aragón (INMA), CSIC – Universidad de Zaragoza, 50009 Zaragoza, Spain.

^cFakultät für Physik, Universität Bielefeld, Postfach 100131, D-33501 Bielefeld, Germany. Email: jschnack@uni-bielefeld.de

^dSchool of Chemistry, The University of Glasgow. Joseph Black Building, Glasgow, G12 8QQ, Scotland, UK. Email: lee.cronin@glasgow.ac.uk

Abstract: The combination of two different Fe^{III} salts in a solvothermal reaction with triethanolamine results in the formation of a high symmetry [Fe^{III}₁₅] cluster whose structure conforms to a centred, tetrakis hexahedron.

Introduction: Homometallic compounds of Fe^{III} have played a central role in the history of molecular magnetism, proving key to the development and understanding of an array of physical properties. For example, the study of oxo-bridged [Fe₂] dimers allowed the development of detailed magneto-structural correlations that can be translated to larger species,¹ antiferromagnetically coupled [Fe₆₋₁₂] ferric wheels revealed interesting quantum size effects manifested in stepped magnetisation,² [Fe_{17/19}] was an early example of a molecule possessing a very large spin ground state,³ [Fe₈] was the second known example of a Single-Molecule Magnet,⁴ [Fe₁₄] was an early example of a compound displaying an enhanced magnetocaloric effect,⁵ and cages ranging in nuclearity from [Fe₁₃] to [Fe₃₄] have structures that conform to Archimedean and Platonic solids which aid understanding of the self-assembly of molecular oxides *en route* to mineral phases.⁶ High symmetry clusters are of particular interest as they may possess geometric spin frustration, a phenomenon whose definition has evolved from its strict initial derivation.⁷ Frustration can lead to some unusual and potentially useful low-temperature physics, a beautiful example being the [Mo₇₂Fe₃₀] icosidodecahedron which shows anomalous magnetisation behaviour in an applied magnetic field.⁸ One synthetic methodology proven to enable the construction of such species is hydro/solvothermal synthesis, which typically exploits superheating reaction solutions under autogenous pressure.⁹ In the chemistry of polynuclear cluster compounds of paramagnetic transition metal ions, the temperature regimes employed (which are typically below 250 °C) can lead to enhanced solubility, reduced solvent viscosity and increased reagent diffusion. The result is often the synthesis of metastable kinetic products of high symmetry, with slow cooling enabling pristine crystal growth directly from the reaction mixture.¹⁰

Results and Discussion: The solvothermal reaction of FeCl₃, Fe(ClO₄)₃·6H₂O and teaH₃ (triethanolamine) in a basic MeOH solution results in the formation of red/brown crystals upon cooling (see the experimental section in the SI for full details). Crystals of [Fe^{III}₁₅O₆(tea)₈Cl₆](ClO₄)₃ (**1**, Fig. 1, S1; Table S1) were found to be in a trigonal crystal system, and structure solution was performed in the R-3 space group (see the crystallographic section in the SI for full details). The metallic skeleton of **1** describes a centred tetrakis hexahedron (Fig. 2), a Catalan solid which is the dual of the truncated octahedron, an Archimedean solid. The central Fe ion (Fe4) is octahedral, being bonded to six oxide ions ([FeO₆]; O5 and symmetry equivalent; Fe-O5 = 1.999 Å). O5 bridges to two further Fe ions in the

peripheral shell ($O_5\text{-Fe}1 = 1.925 \text{ \AA}$; $O_5\text{-Fe}2 = 2.025 \text{ \AA}$) and is thus three coordinate and trigonal planar. There is a fourth, longer contact to $\text{Fe}3$ ($O_5\text{-Fe}3 = 2.492 \text{ \AA}$), so O_5 may be considered pseudo-tetrahedral if one considers this interaction significant (Fig. 2, S2-3). The outer shell is decorated with a combination of halide and tea^{3-} ions. The former are monodentate, coordinated to $\text{Fe}2$ ($\text{Fe}2\text{-Cl}, 2.315 \text{ \AA}$). The latter are tetradentate, chelating either $\text{Fe}1$ or $\text{Fe}3$ with each O-atom μ -bridging to a second Fe ion ($\text{Fe}2$). Thus $\text{Fe}1$ is five-coordinate ($[\text{FeO}_4\text{N}]$) and trigonal pyramidal, $\text{Fe}2$ is six-coordinate ($[\text{FeO}_5\text{Cl}]$) and octahedral, and $\text{Fe}3$ is four coordinate($[\text{FeO}_3\text{N}]$) and trigonal prismatic, or seven coordinate ($[\text{FeO}_6\text{N}]$) and a capped octahedron if the Fe-O_5 bonds are included (Fig. S3-4). A review of the Cambridge Structural Database (CSD) for Fe-O bond lengths in any Fe-O-Fe moiety produces 3378 different compounds and 12361 bond lengths ranging from a minimum value of 1.651 \AA to a maximum value of 2.629 \AA , as depicted in the histogram in Fig. S5. The $[\text{Fe}_{15}\text{O}_{30}]$ core displays a breadth of different Fe-O-Fe angles, ranging from a minimum of 86.67° ($\text{Fe}4\text{-O}_5\text{-Fe}3$) to a maximum of 140.82° ($\text{Fe}4\text{-O}_5\text{-Fe}2$). Angles from the central $\text{Fe}4$ ion to the peripheral $\text{Fe}1$ and $\text{Fe}2$ ions via the O_5 oxide are 140.82° and 117.41° , while those connecting the outer $\text{Fe}1$, $\text{Fe}2$ and $\text{Fe}3$ ions together via the oxides and alkoxides range between $86.7\text{-}129.39^\circ$ (Table S2). The closest intermolecular interactions are between the monodentate Cl ions on $\text{Fe}2$ and the C-atoms of the tea^{3-} ligands on neighbouring molecules ($\text{Cl}1\ldots\text{C}7, \sim 3.43 \text{ \AA}$), and between the perchlorate O-atoms and the C-atoms of the tea^{3-} ligands ($\text{O}_6\ldots\text{C}4, \sim 3.43 \text{ \AA}$; Fig. S6-7). This results in an aesthetically pleasing honeycomb-like network when viewed down the c -axis of the cell. A search of the CSD reveals that just three $[\text{Fe}_{15}]$ clusters have been reported previously,¹¹ with **1** being the first example of a [centred] tetrakis hexahedron. Perhaps more surprisingly, given the widespread use of the H_3tea ligand in 3d coordination chemistry, there are very few homometallic Fe^{III} clusters of this ligand deposited. Indeed, they are limited to $[\text{Fe}_5]$,¹² $[\text{Fe}_6]$ wheels (both unsupported¹³ and supported¹⁴), $[\text{Fe}_7]$,¹⁵ $[\text{Fe}_8]$ ¹⁶ (including an $[\text{Fe}_8]$ cluster self-assembled into a $[\text{Fe}_{64}]$ cage¹⁷), and $[\text{Fe}_{10}]$.¹⁸ Heterometallic Fe-Ln species are far more prevalent.¹⁹

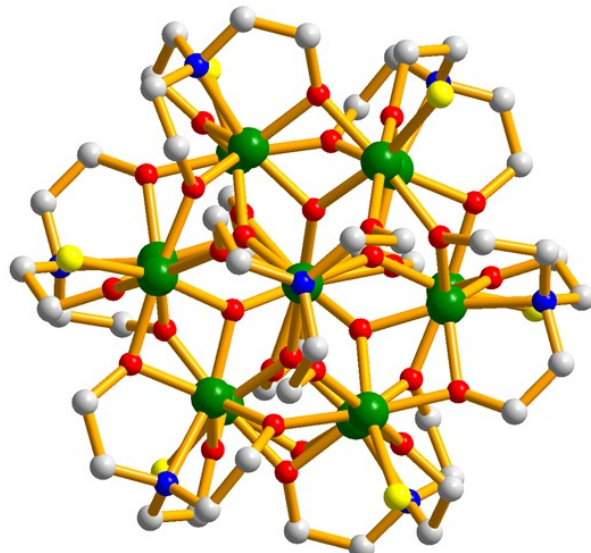


Figure 1. Molecular structure of the cation of **1** viewed down the c -axis of the unit cell. Colour code: $\text{Fe} = \text{green}$, $\text{O} = \text{red}$, $\text{N} = \text{blue}$, $\text{C} = \text{grey}$, $\text{Cl} = \text{yellow}$. H atoms omitted for clarity.

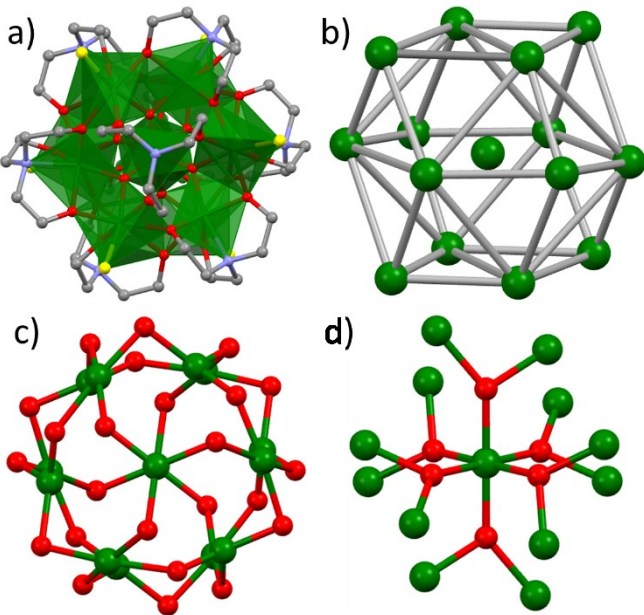


Figure 2. Different views of the structure of the cation of **1**. a) The molecular structure of the cation of **1** viewed down the *c*-axis of the unit cell with the metal ions drawn in polyhedral format. b) The metallic skeleton, which conforms to a [centred] tertrakis hexahedron. The $[M_{15}O_6]^{33+}$ metal-oxide core, highlighting c) the Fe-O connectivity in the outer shell of the molecule via the bridging alkoxides, and d) the link between the central Fe ion and the outer shell via the six μ_3 -oxide ions. Fe = green, O = red, n = blue, C = grey, Cl = yellow. H atoms omitted for clarity.

The direct-current (dc) molar magnetic susceptibility, χ , of a polycrystalline sample of **1** was measured in an applied magnetic field, B , of 0.1 T, over the 2–300 K temperature, T , range. The results are plotted in Fig. 3 in the form of χT product, where $\chi = M / B$ with M the magnetisation. At room temperature, the χT product is 28.67 emu K mol⁻¹, much lower than the Curie constant expected for fifteen uncorrelated $S = 5/2$ centres (65.625 emu K mol⁻¹) with $g = 2$. On lowering the temperature, the χT product decreases rapidly, reaching a value of 11.05 emu K mol⁻¹ at $T = 10$ K, before decreasing even more abruptly to a value of 7.74 emu K mol⁻¹ at $T = 2$ K. The data suggest a ground state spin of $S \approx 9/2$ (compare arrows in Fig. 3). Variable-temperature-variable-field (VTVB) dc magnetisation measurements in the temperature range 2–6 K and in applied magnetic fields up to 7 T reach a maximum value of just $M = 8.35 \mu_B$ (Fig. 3b), well below the upper limit expected for a ferromagnetically coupled system ($M = 75 \mu_B$ for $g = 2$). This behaviour is clearly indicative of relatively strong antiferromagnetic interactions between the Fe^{III} ions, consistent with the Fe-O distances and Fe-O-Fe angles present.¹

It is computationally impossible to quantitatively analyse the magnetic data of a molecule containing $15 \times S = 5/2$ spins *via* conventional matrix diagonalisation techniques since the dimension of the Hilbert space is 470,184,984,576, and thus we turn to the finite-temperature Lanczos method.²⁰ Even here, several assumptions must be made. (A) Despite the presence of eight independent exchange interactions, we reduce this to four based on similar Fe-O bond lengths and Fe-O-Fe angles (Fig. S8). These are: J_{cube} along edges of the cube; J_{pyramid} along the four edges from the top of each pyramid to the respective base square of cube; $J_{c,\text{cube}}$ from central Fe inside the cube to vertices of the cube; and $J_{c,\text{pyramid}}$ from central Fe ion to the tops of pyramids. (B) We simulate the data using isotropic $S = 3/2$ spins rather than isotropic $S = 5/2$ spins and scale the resulting data accordingly. The corresponding isotropic spin-Hamiltonian is:

$$\hat{H} = -2 \sum_{i < j} J_{ij} \hat{\vec{s}}_i \cdot \hat{\vec{s}}_j , \text{ where } J_{ij} \text{ denotes the four employed exchange constants, respectively.}$$

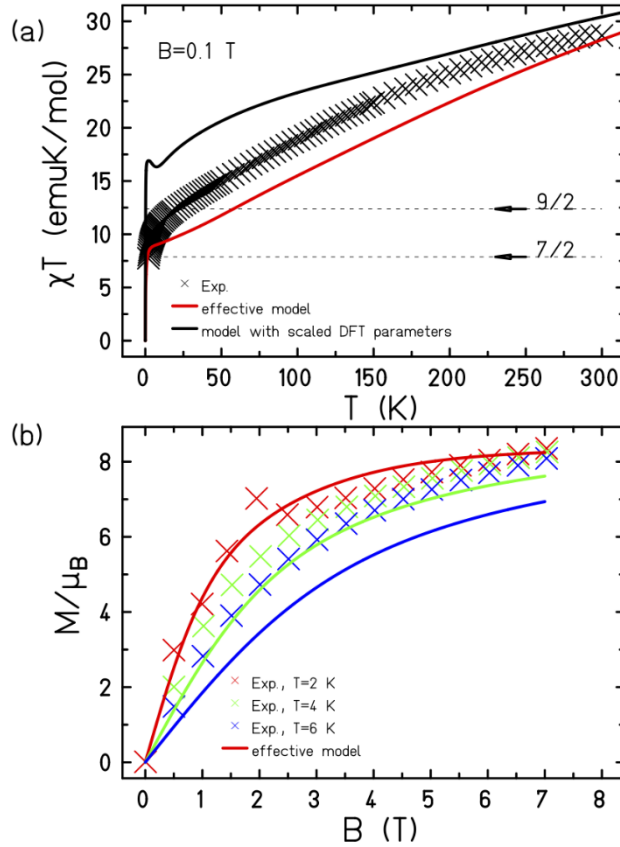


Figure 3. (a) Magnetic susceptibility (χT) versus temperature (T) data for **1** measured in an applied field, $B = 0.1$ T in the $T = 300\text{-}1.80$ K temperature range. (b) Magnetisation (M) versus field (B) data in the 2-6 K temperature and and 0-7 T field ranges. The solid lines are a simulation of the experimental data (x) using the finite-temperature Lanczos method. The effective model denotes a Heisenberg model with high symmetry, as described in the main text. The black line in (a) denoted the model employing DFT parameters given in Table S3 in a Heisenberg model scaled by 25/9 taking into account the use of spins, $S = 3/2$.

A rather good theoretical representation of the data (Fig. 3) was obtained with $J_{\text{cube}} = -17.4 \text{ cm}^{-1}$, $J_{\text{pyramid}} = -17.4 \text{ cm}^{-1}$, $J_{c,\text{cube}} = -17.4 \text{ cm}^{-1}$ and $J_{c,\text{pyramid}} = -3.5 \text{ cm}^{-1}$, scaled by 9/25 to meet a Hamiltonian with spins $S = 5/2$. Such a scaling approach can only provide “an order of magnitude” estimate of the exchange constants, rather than a precise derivation, albeit the numbers are entirely consistent with experimentally and computationally derived magneto-structural correlations for O-bridged Fe^{III} clusters.²¹ The exchange constants are indicative of a highly frustrated system, as one might expect from the structural symmetry. Heat capacity, C , measurements were collected between ~ 0.3 K and 30 K, for $B = 0, 3$ and 7 T (Fig. S9). Below ~ 3 K, the heat capacity depends significantly on B , the zero-field C showing essentially flat behaviour and reaching values close to $\sim 0.5R$, where R is the gas constant. This behaviour is similar to that recently reported for an [Fe^{III}₁₀Gd^{III}₁₀] wheel²² and consistent with the presence of a large density of low-lying states, likely resulting from competing antiferromagnetic interactions.

To further support the relative sign and magnitude of the coupling constants obtained, we have performed DFT calculations (see the SI for the computational details) on a model complex, **1A**, derived from complex **1** (Figure S10-11). These suggest that the eight independent exchange interactions are

in the range $|J| = 4.6\text{-}16.4 \text{ cm}^{-1}$ (Table S3), in good agreement with the experimental simulations. All are antiferromagnetic in nature, with the exception of the $\text{Fe}_4\text{-}(\mu_4\text{-O}^{2-})_3\text{-Fe}_3$ interaction which affords $J = +4.6 \text{ cm}^{-1}$ on account of the large Fe-O bond lengths and small Fe-O-Fe bond angles present which lead to orbital orthogonality. Overlap integral calculations²³ using metal-based singly occupied molecular orbitals (SOMOs) reveal that the strongest antiferromagnetic interactions occur where there are a higher number of strong or moderate overlap integrals, and vice versa (Fig. S12-13). For the $\text{Fe}_4\text{-}(\mu_4\text{-O}^{2-})_3\text{-Fe}_3$ interaction (J_1 in Table S3-4) there is only one strong interaction ($d_z^2 \parallel d_{xz}$) with the remaining 24 interactions being weak. The overall result is a weak/moderate ferromagnetic interaction. Spin density analysis suggests that strong spin delocalisation is present in **1** with Fe^{II} spin densities ranging between 4.007-4.151 (Fig. S14).

Conclusions: It is somewhat unusual for synthetic chemists to employ two different metal salts for the formation of homometallic cluster compounds containing paramagnetic 3d metals, since the anions are often considered solely as charge balancing moieties rather than structure-directing agents. This observation has certainly prompted us to re-examine a number of reactions to probe whether it may be of general applicability, or if it is of more limited scope. Here, the use of both FeCl_3 , $\text{Fe}(\text{ClO}_4)_3\cdot6\text{H}_2\text{O}$ with teaH_3 in a high temperature, high pressure reaction leads to the formation of an aesthetically pleasing $[\text{Fe}_{15}]$ cage conforming to a centred, tetrakis hexahedron. The high symmetry of the metallic skeleton leads to the presence of competing antiferromagnetic exchange interactions and spin frustration. Use of the finite temperature Lanczos method allows for “an order of magnitude” estimation of the exchange constants present, a computationally non-trivial task for a molecule containing fifteen $S = 5/2$ spins. Values of $J_{\text{cube}} = -17.4 \text{ cm}^{-1}$, $J_{\text{pyramid}} = -17.4 \text{ cm}^{-1}$, $J_{c,\text{cube}} = -17.4 \text{ cm}^{-1}$ and $J_{c,\text{pyramid}} = -3.5 \text{ cm}^{-1}$ are consistent with parameters obtained from DFT calculations which fall in the range $|J| = 4.6\text{-}16.4 \text{ cm}^{-1}$, and with low temperature heat capacity data which reflects the presence of a large density of low-lying spin states.

Author Contributions: DJC performed the synthesis and measured the SQUID data, MKS performed the theoretical studies, DJC and GSN measured and solved the structural data, ME collected and analysed the heat capacity data, JS analysed the magnetic data, LC and EKB conceived the idea, and all authors contributed to writing and editing the manuscript.

Acknowledgements: EKB and LC thank U21/EPSRC for funding a studentship (DJC). MKS would like to thank Edinburgh Compute and Data Facility (ECDF), and the European Union Horizon 2020 research and innovation programme under the Marie Skłodowska-Curie grant agreement No. 832488. ME thanks the Spanish Ministry of Science and Innovation (Project RTI2018-098537-B-C22).

References

1. H. Weihe and H. U. Güdel, *J. Am. Chem. Soc.*, 1998, **120**, 2870-2879; C. Cañada-Vilalta, T. A. O'Brien, E. K. Brechin, M. Pink, E. R. Davidson and G. Christou, *Inorg. Chem.*, 2004, **43**, 5505-5521.
2. R. W. Saalfrank, I. Bernt, E. Uller and F. Hampel, *Angew. Chem., Int. Ed. Engl.*, 1997, **36**, 2482-2485; A. Caneschi, A. Cornia and S. J. Lippard, *Angew. Chem. Int. Ed. Engl.*, 1995, **34**, 467-469; K. L. Taft, C. D. Delfs, G. C. Papaefthymiou, S. Foner, D. Gatteschi and S. J. Lippard, *J. Am. Chem. Soc.*, 1994, **116**, 823-832; A. Caneschi, A. Cornia, A. C. Fabretti and D. Gatteschi, *Angew. Chem. Int. Ed.*, 1999, **38**, 1295-1297.
3. A. K. Powell, S. L. Heath, D. Gatteschi, L. Pardi, R. Sessoli, G. Spina, F. Del Giallo and F. Pieralli, *J. Am. Chem. Soc.*, 1995, **117**, 2491-2502.

4. C. Delfs, D. Gatteschi, L. Pardi, R. Sessoli, K. Wieghardt and D. Hanke, *Inorg. Chem.*, 1993, **32**, 3099–3103.
5. R. Shaw, R. H. Laye, L. F. Jones, D. M. Low, C. Talbot-Eeckelaers, Q. Wei, C. J. Milios, S. Teat, M. Helliwell, J. Raftery, M. Evangelisti, M. Affronte, D. Collison, E. K. Brechin and E. J. L. McInnes, *Inorg. Chem.*, 2007, **46**, 4968–4978.
6. A. Bino, M. Ardon, D. Lee, B. Spingler and S. J. Lippard, *J. Am. Chem. Soc.*, 2002, **124**, 4578–4579; O. Sadeghi, L. N. Zakharov and M. Nyman, *Science*, 2015, **347**, 1359–1362; C. Vecchini, D. H. Ryan, L. M. D. Cranswick, M. Evangelisti, W. Kockelmann, P. G. Radaelli, A. Candini, M. Affronte, I. A. Gass, E. K. Brechin and O. Moze, *Phys. Rev. B*, 2008, **77**, 224403; O. Nachtigall, M. Kusserow, R. Clérac, W. Wernsdorfer, M. Menzel, F. Renz, J. Mrozinski and J. Spandl, *Angew. Chem. Int. Ed.*, 2015, **54**, 10361–10364; A. E. Dearle, D. J. Cutler, H. W. L. Fraser, S. Sanz, E. Lee, S. Dey, I. F. Diaz-Ortega, G. S. Nichol, H. Nojiri, M. Evangelisti, G. Rajaraman, J. Schnack, L. Cronin and E. K. Brechin, *Angew. Chem. Int. Ed.*, 2019, **58**, 16903–16906; N. A. G. Bandeira, O. sadeghi, T. J. Woods, Y.-Z. Zhang, J. Schnack, K. Dunbar, M. Nyman and X. Bo., *J. Phys. Chem. A*, 2017, **121**, 1310 – 1318.
7. G. Toulouse, *Comm. Phys.*, 1977, **2**, 115–119; S. Kirkpatrick, *Phys. Rev. B*, 1977, **16**, 4630–4641; c) A. P. Ramirez, *Annu. Rev. Mater. Sci.*, 1994, **24**, 453; O. Kahn, *Chem. Phys. Lett.*, 1997, **265**, 109–114; C. Schröder, H. Nojiri, J. Schnack, P. Hage, M. Luban and P. Kögerler, *Phys. Rev. Lett.*, 2005, **94**, 017205; J. Schnack, *Dalton Trans.*, 2010, **39**, 4677–4686; M. L. Baker, G. A. Timco, S. Piligkos, J. S. Mathieson, H. Mutka, F. Tuna, P. Kozłowski, M. Antkowiak, T. Guidi, T. Gupta, H. Rath, R. J. Woolfson, G. Kamieniarz, R. G. Pritchard, H. Weihe, L. Cronin, G. Rajaraman, D. Collison, E. J. L. McInnes and R. E. P. Winpenny, *Proc. Natl. Acad. Sci.*, 2012, **109**, 19113–19118.
8. V. O. Garlea, S. E. Nagler, J. L. Zarestky, C. Stassis, D. Vaknin, P. Kögerler, D. F. McMorrow, C. Niedermayer, D. A. Tennant, B. Lake, Y. Qiu, M. Exler, J. Schnack and M. Luban, *Phys. Rev. B*, 2006, **73**, 024414.
9. M. I. Khan, J. Zubieta, *Prog. Inorg. Chem.*, 1995, **43**, 1-149.
10. R. H. Laye and E. J. L. McInnes, *Eur. J. Inorg. Chem.*, 2004, 2811-2818 .
11. Y. Hou, X. Fang, K. D. Kwon, L. J. Criscenti, D. Davis, T. Lambert and M. Nyman, *Eur. J. Inorg. Chem.*, 2013, 1780–1787; E. Freire, M. Quintero, D. Vega and R. Baggio, *Inorg. Chim. Acta*, 2013, **394**, 229–236; A.-Q. Zhang and L.-L. Liu, *Transit. Met. Chem.*, 2017, **42**, 753–761.
12. W. Schmitt, L. Zhang, C. E. Anson and A. K. Powell, *Dalton Trans.*, 2010, **39**, 10279–10285.
13. A. Baniodeh, Y. Liang, C. E. Anson, N. Magnani, A. K. Powell, A.-N. Unterreiner, S. Seyfferle, M. Slota, M. Dressel, L. Bogani and K. Goß, *Adv. Funct. Mater.*, 2014, **24**, 6280–6290.
14. R. W. Saalfrank, I. Bernt, E. Uller and F. Hampel, *Angew. Chem. Int. Ed.*, 1997, **36**, 2482-2485.
15. L. F. Jones, P. Jensen, B. Moubaraki, K. J. Berry, J. F. Boas, J. R. Pilbrow and K. S. Murray, *J. Mater. Chem.*, 2006, **16**, 2690–2697.
16. O. Waldmann, R. Koch, S. Schromm, J. Schülein, P. Müller, I. Bernt, R. W. Saalfrank, F. Hampel and E. Balthes, *Inorg. Chem.*, 2001, **40**, 2986-2995; G. Xiong, Y.-L. Hou, J.-Z. Cui and B. Zhao, *Inorg. Chem. Commun.*, 2013, **35**, 89-61; A. M. Ako, O. Waldmann, V. Mereacre, F. Klöwer, I. J. Hewitt, C. E. Anson, H. U. Güdel and A. K. Powell, *Inorg. Chem.*, 2007, **46**, 756–766; O. Botezat, J. van Leusen, V. Ch. Kravtsov, A. Ellern, P. Kögerler and S. G. Baca, *Dalton Trans.*, 2015, **44**, 20753-20762; I. A. Gass, C. J.

- Milios, A. Collins, F. J. White, L. Budd, S. Parsons, M. Murrie, S. P. Perlepes and E. K. Brechin, *Dalton Trans.*, 2008, 2043–2053; M. Murugesu, K. A. Abboud and G. Christou, *Dalton Trans.*, 2003, 4552-4556.
17. T. Liu, Y.-J. Zhang, Z.-M. Wang and S. Gao, *J. Am. Chem. Soc.*, 2008, **130**, 10500-10501.
18. S.-J. Liu, S.-D. Han, J.-M. Jia, L. Xue, Y. Cui, S.-M. Zhang and Z. Chang, *CrystEngComm.*, 2014, **16**, 5212-5215.
19. M. Murugesu, A. Mishra , W. Wernsdorfer , K. A. Abboud and G. Christou, *Polyhedron*, 2006, **25** , 613 —625; O. Botezat, J. van Leusen, V. Ch. Kravtsov, P. Kögerler and S. G. Baca, *Inorg. Chem.*, 2017, **56**, 1814–1822.
20. J. Jaklič, P. Prelovšek, *Phys. Rev. B*, 1994, **49**, 5065-5068; J. Schnack, O. Wendland, *Eur. Phys. J. B*, 2010, **78**, 535-541; J. Schnack, J. Richter, R. Steinigeweg, *Phys. Rev. Research*, 2020, **2**, 013186.
21. M. K. Singh and G. Rajaraman, *Inorg. Chem.*, 2019, **58**, 3175-3188; K. J. Mitchell, K. A. Abboud and G. Christou, *Inorg. Chem.*, 2016, **55**, 6597.
22. A. Baniodeh, N. Magnani, Y. Lan, G. Butth, C. E. Anson, J. Richter, M. Affronte, J. Schnack and A.K. Powell, *npj Quant. Mater.*, 2018, **3**, 10.
23. M. Coletta, S. Sanz, D. J. Cutler, S. J. Teat, K. J. Gagnon, M. K. Singh, E. K. Brechin and S. J. Dalgarno, *Dalton Trans.*, 2020, **49**, 14790-14797; M. Coletta, T. G. Tziotzi, M. Gray, G. S. Nichol, M. K. Singh, C. J. Milios and E. K. Brechin, *Chem. Commun.*, 2021, **57**, 4122-4125; S. Hazra, S. Bhattacharya, M. K. Singh, L. Carrella, E. Rentschler, T. Weyhermueller, G. Rajaraman and S. Mohanta, *Inorg. Chem.*, 2013, **52**, 12881-12892

Supporting Information

Experimental Details

Synthetic procedure

Synthesis of $[\text{Fe}_{15}\text{O}_6(\text{tea})_8\text{Cl}_6](\text{ClO}_4)_3$ (1)

FeCl_3 (0.162 g, 1 mmol) and $\text{Fe}(\text{ClO}_4)_2 \cdot 6\text{H}_2\text{O}$ (0.254 g, 1 mmol) were dissolved in methanol (25 cm^3). Triethanolamine (0.198 cm^3 , 1.5 mmol) was added dropwise to the orange solution. Triethylamine (0.418 cm^3 , 3 mmol) was added dropwise and the darkened solution was stirred at room temperature overnight. The dark orange solution was then filtered under gravity and 12.5 cm^3 samples of the filtrate were transferred to Teflon-lined autoclaves and heated to 100°C for 24 hrs. the reaction vessels were left to cool and stand for 48 hrs yielding dark red rod-shaped crystals suitable for X-ray Diffraction. Yield =0.096 g [0.041 mmol] (31.5% by Fe). Elemental analysis (% C H N) calculated (found) for $\text{C}_{48}\text{H}_{96}\text{Cl}_8\text{Fe}_{15}\text{N}_8\text{O}_{38}$: C 24.9 (24.35), H 4.18 (4.28), N 4.84 (4.40).

Single Crystal X-ray Diffraction

Diffraction data for **1** was collected using a Oxford Diffraction Xcalibur diffractometer with Mo $\text{K}\alpha$ radiation, and is given in Table S1. An Oxford Cryosystems Cryostream 700+ low temperature device was used to maintain a crystal temperature of 120.0 K. The structure was solved using ShelXT and refined with version ShelXL interfaced through Olex2.^{1,2} All non-hydrogen atoms were refined using anisotropic displacement parameters. H atoms were placed in calculated positions geometrically and refined using the riding model. CCDC = 2090901.

Compound (1)			
Formula	$\text{C}_{48}\text{H}_{96}\text{Cl}_8\text{Fe}_{15}\text{N}_8\text{O}_{38}$	Z'	0.166667
$D_{\text{calc.}}/\text{g cm}^{-3}$	2.000	Wavelength/ \AA	0.71073
μ/mm^{-1}	2.864	Radiation type	Mo $\text{K}\alpha$
Formula Weight	2514.67	$\Theta_{\min}/^\circ$	3.363
Colour	dark red	$\Theta_{\max}/^\circ$	29.352
Shape	block-shaped	Measured Refl's.	15300
Size/mm ³	$0.80 \times 0.50 \times 0.30$	Indep't Refl's	3385
T/K	120.0(2)	Refl's $I \geq 2 \sigma(I)$	2914
Crystal System	trigonal	R_{int}	0.0219
Space Group	$R\bar{3}$	Parameters	292
$a/\text{\AA}$	15.1578(5)	Restraints	275
$b/\text{\AA}$	15.1578(5)	Largest Peak	1.629
$c/\text{\AA}$	31.4738(12)	Deepest Hole	-1.460
$\alpha/^\circ$	90	GooF	1.122
$\beta/^\circ$	90	wR_2 (all data)	0.1541
$\gamma/^\circ$	120	wR_2	0.1484
$V/\text{\AA}^3$	6262.6(5)	R_1 (all data)	0.0771
Z	3	R_1	0.0661

Table S1. Single crystal X-ray diffraction data for complex **1**.

Powder X-ray Diffraction

Diffraction data were collected on polycrystalline powders using a Bruker D2 PHASER with nickel filtered Cu radiation at power 30 kW and current 10mA. Diffraction measured from $2\theta = 5^\circ - 50.021^\circ$; step size, 0.0162°; time per step, 0.525 s.

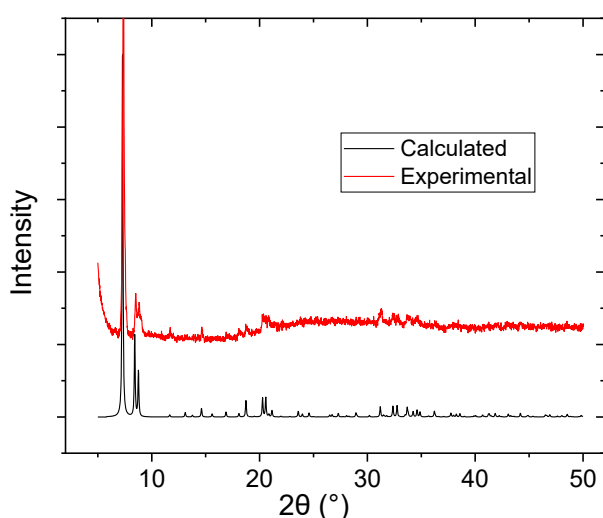


Figure S1. Powder X-ray diffraction of **1**. Experimental data (red) and calculated (black) data.

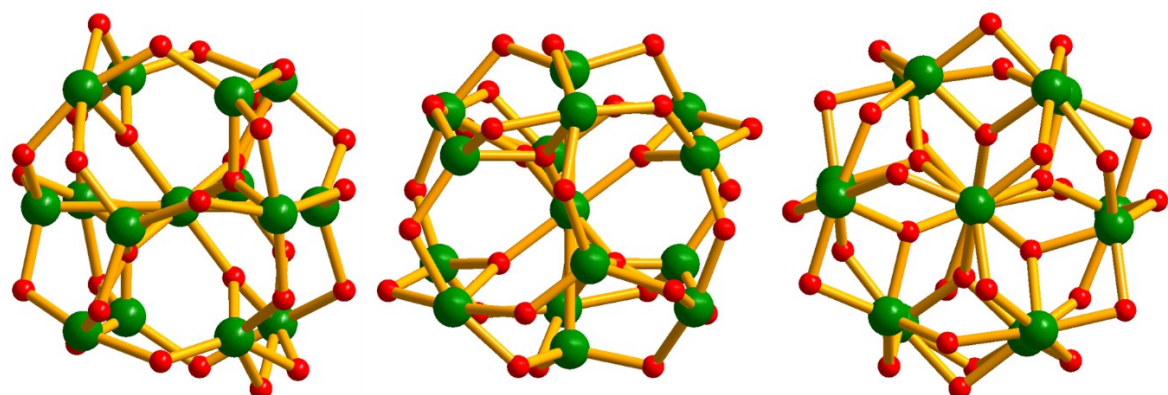


Figure S2. Orthogonal views of the metal-oxygen core of **1**, down the (left to right) *a*-, *b*- and *c*-axis of the unit cell.

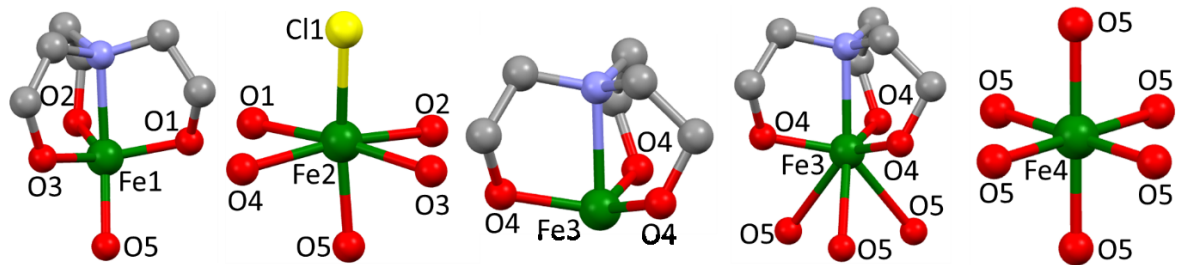


Figure S3. Metal coordination at the four symmetry inequivalent Fe ions. Fe1 = five coordinate, trigonal pyramidal; Fe2 = six coordinate, octahedral; Fe3 = four coordinate, trigonal prism or seven coordinate, capped octahedron if the Fe-O5 bonds are included; Fe4 = octahedral. Colour code: Fe = green, O = red, N = blue, C = grey, Cl = yellow. H-atoms omitted.

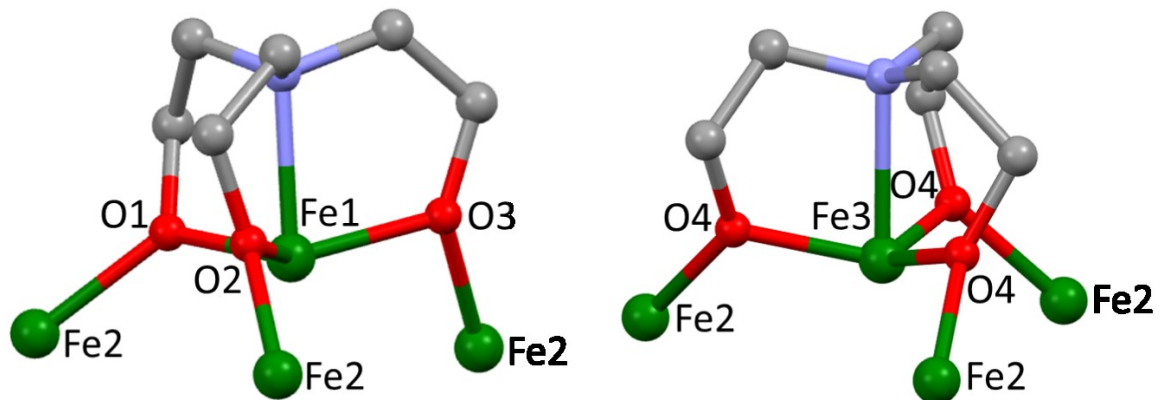


Figure S4. Coordination/bridging mode of the tea^{3-} ligands bonded to Fe1 and Fe3. Colour code: Fe = green, O = red, N = blue, C = grey. H-atoms omitted.

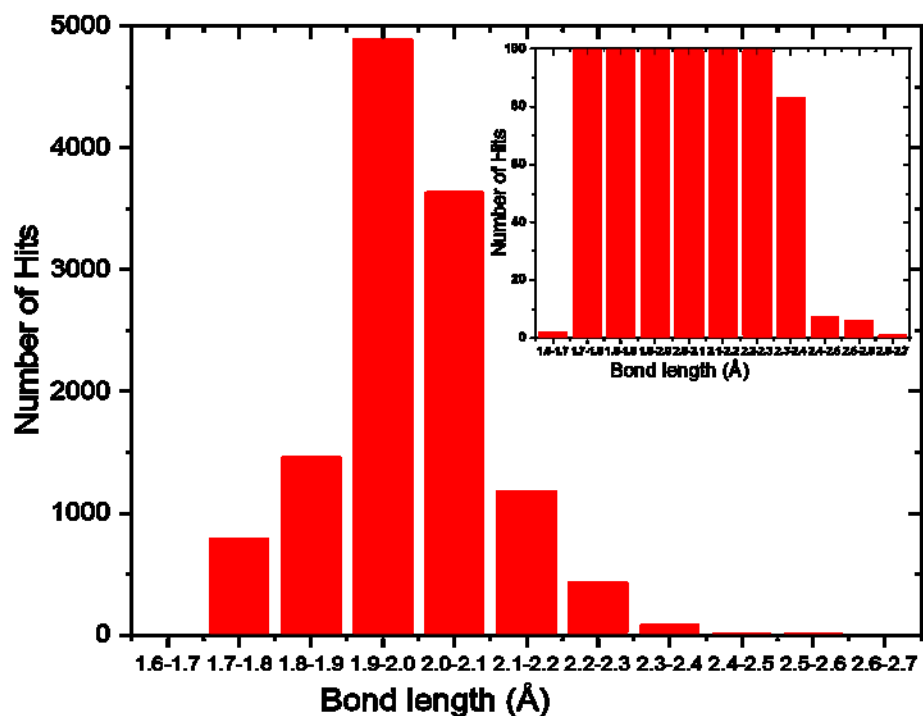


Figure S5. Histogram showing the hits resulting from a bond length search of the Cambridge Structural Database for compounds containing the Fe-O-Fe moiety, with no other restrictions. There are a total of 3378 compounds and 12361 Fe-O bonds. The shortest bond length is 1.651 Å and the longest bond length is 2.629 Å.

Atom	Atom	Length/Å	Atom	Atom	Atom	Angle/°
Fe1	O1	1.824(8)	Fe1	O1	Fe2	129.4(4)
Fe1	O2	1.986(10)	Fe1	O2	Fe2	116.7(4)
Fe1	O3	1.976(9)	Fe1	O3	Fe2	98.4(3)
Fe1	O5	1.925(4)	Fe1	O5	Fe2	99.8(18)
Fe1	N1	2.226(5)	Fe1	O5	Fe4	117.4(19)
Fe2	Cl1	2.315(15)	Fe3	O4	Fe2	112.9(3)
Fe2	O1	2.047(8)	Fe3	O5	Fe4	86.7(4)
Fe2	O2	1.996(9)	Fe4	O5	Fe2	140.8(2)
Fe2	O3	2.015(8)				
Fe2	O4	1.978(7)				
Fe2	O5	2.025(4)				
Fe3	O4	1.917(7)				
Fe3	O5	2.492(9)				
Fe3	N2	2.336(8)				
Fe4	O5	1.999(4)				

Table S2. Pertinent bond lengths (Å) and angles (°) for **1**.

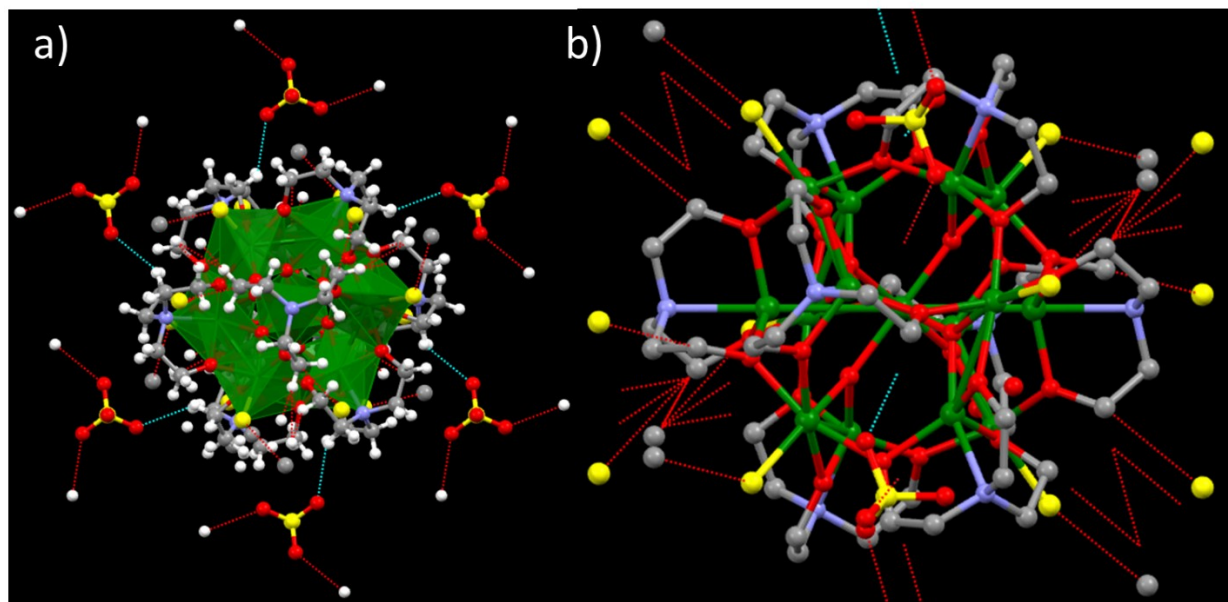


Figure S6. Closest intermolecular interactions between the perchlorate O-atoms and the C-atoms of the tea^{3-} ligands as viewed down the c -axis of the unit cell (a), and between the Cl ions and the C-atoms of the tea^{3-} ligands as viewed down the b -axis of the unit cell (b), at distances of $\sim 3.4 \text{ \AA}$. Colour code: Fe = green, O = red, N = blue, C = grey, Cl = yellow, H = white.

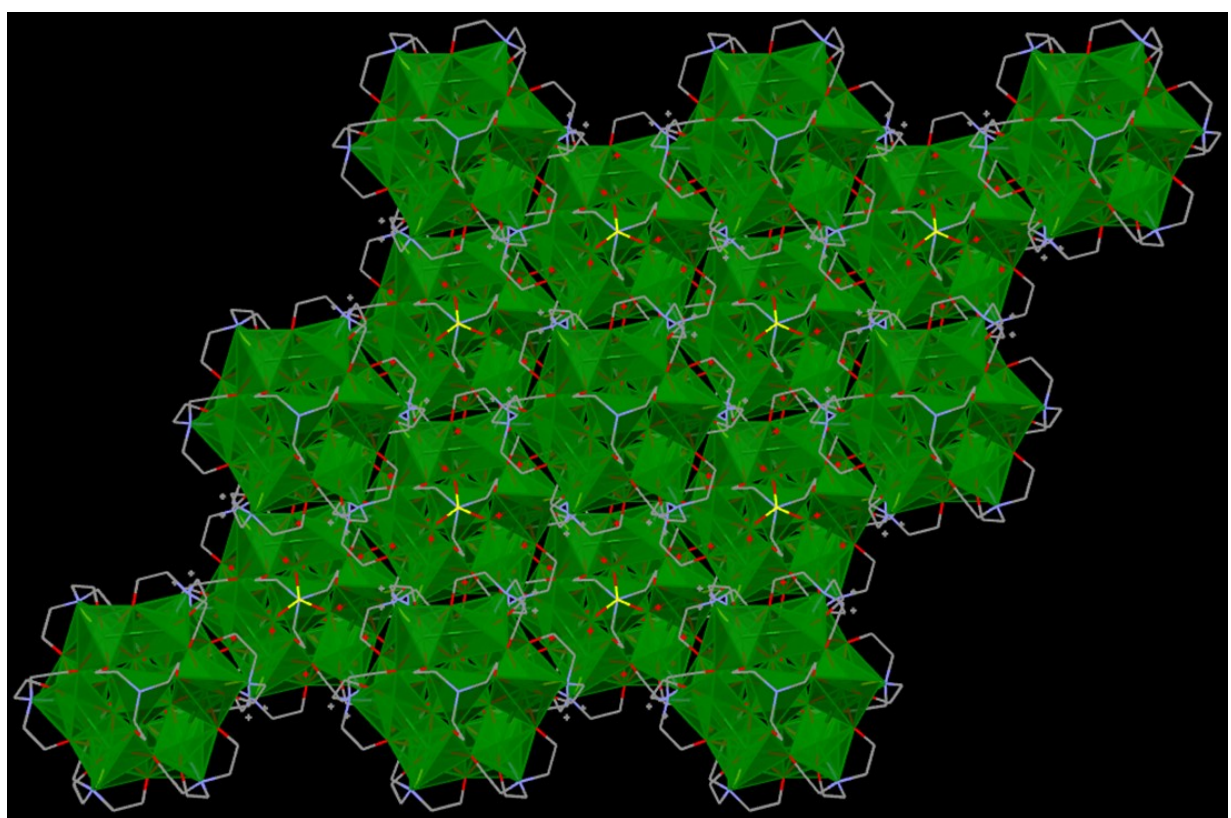


Figure S7. Packing of **1** in the extended structure, viewed down the c -axis of the unit cell. The Fe ions are given in polyhedral format. Colour code: Fe = green, O = red, N = blue, C = grey, Cl = yellow. H-atoms omitted.

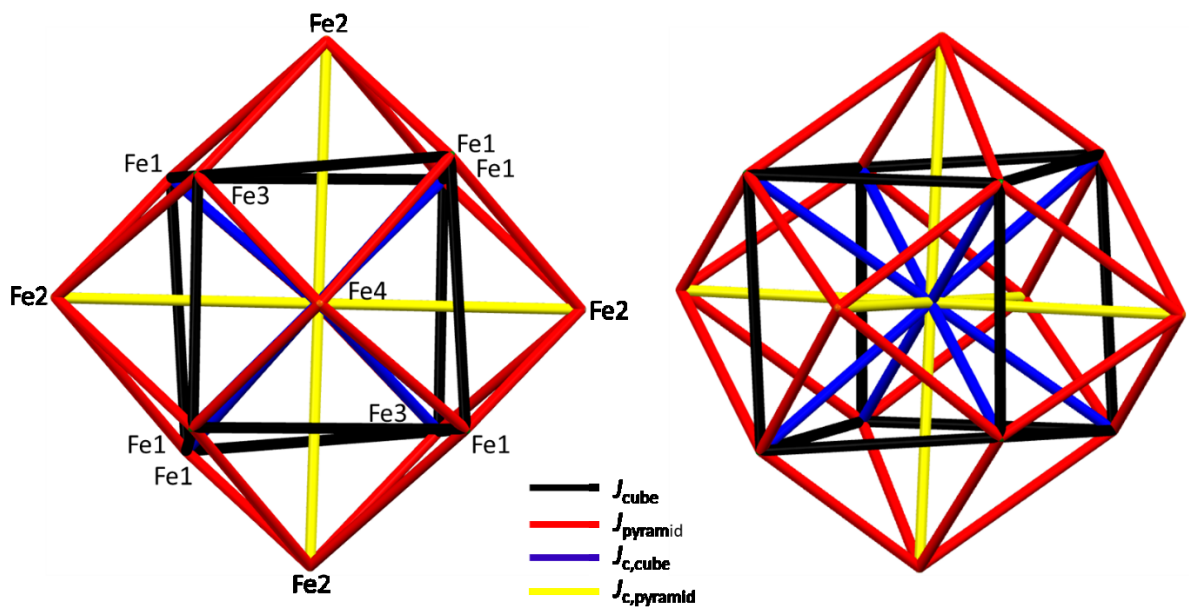


Figure S8. Exchange interaction scheme employed to simulate the magnetic susceptibility and magnetisation data of **1** using four J values (inset) and the finite temperature Lanczos method. The two figures show different orientations of the same scheme for clarity.

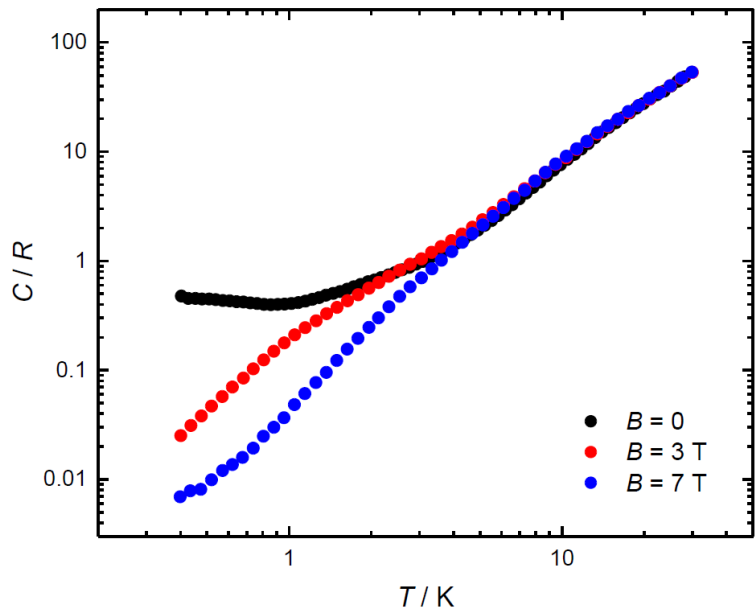


Figure S9. Heat capacity data for **1** in the indicated temperature and field ranges.

Computational details:

Based on symmetry and structural parameters, there are a total of eight unique magnetic exchange interactions (J_1 - J_8) present in **1**. These interactions are estimated using density functional theory (DFT) in the Gaussian 16 suite on model complex **1A** derived from **1** (Fig. S10).³ We have used the diamagnetic substitution method where we keep only the two paramagnetic Fe^{III} ions of interest and replace all others paramagnetic Fe^{III} metal ions with diamagnetic Ga^{III} ions. This method is known to be reliable for molecular systems with moderate magnetic exchange interactions.⁴⁻⁶ Noddleman's broken symmetry approach⁷ is used to calculate the magnetic exchange coupling constants. The B3LYP functional⁸⁻¹⁰ along with Ahlrichs TZV basis set¹¹⁻¹³ is used for Fe, Ga; and the 6-31G* basis set¹⁴ for Cl, O, N, C and H to estimate the magnetic exchange coupling constants. The methodology is known to reproduce the experimental J values for 3d metal clusters.^{5-6, 15-24}

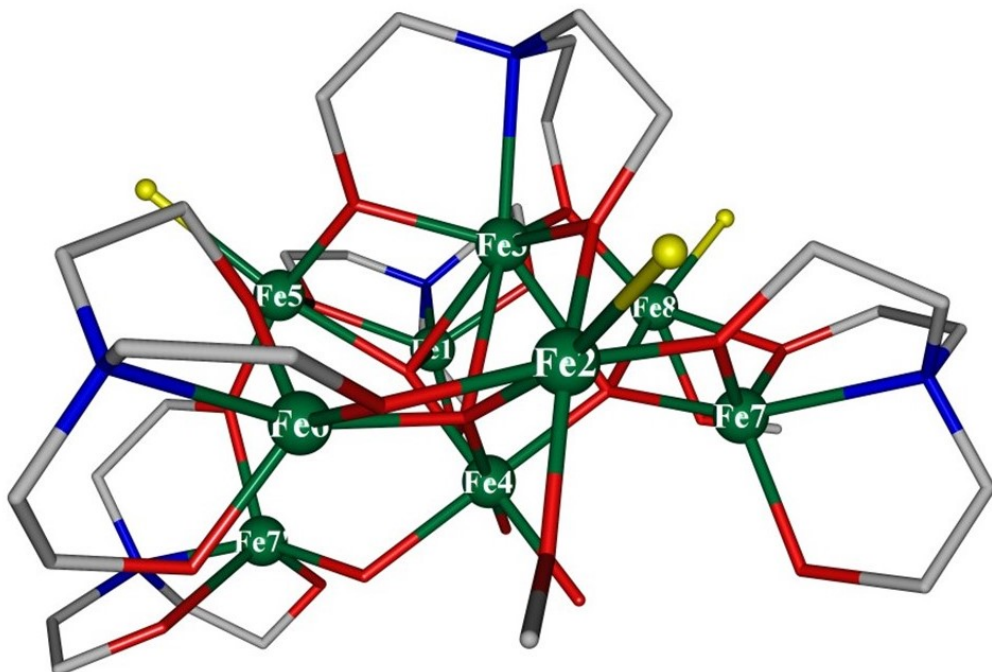


Figure S10. Model complex **1A** derived from **1**. Colour code as in Figure 2.

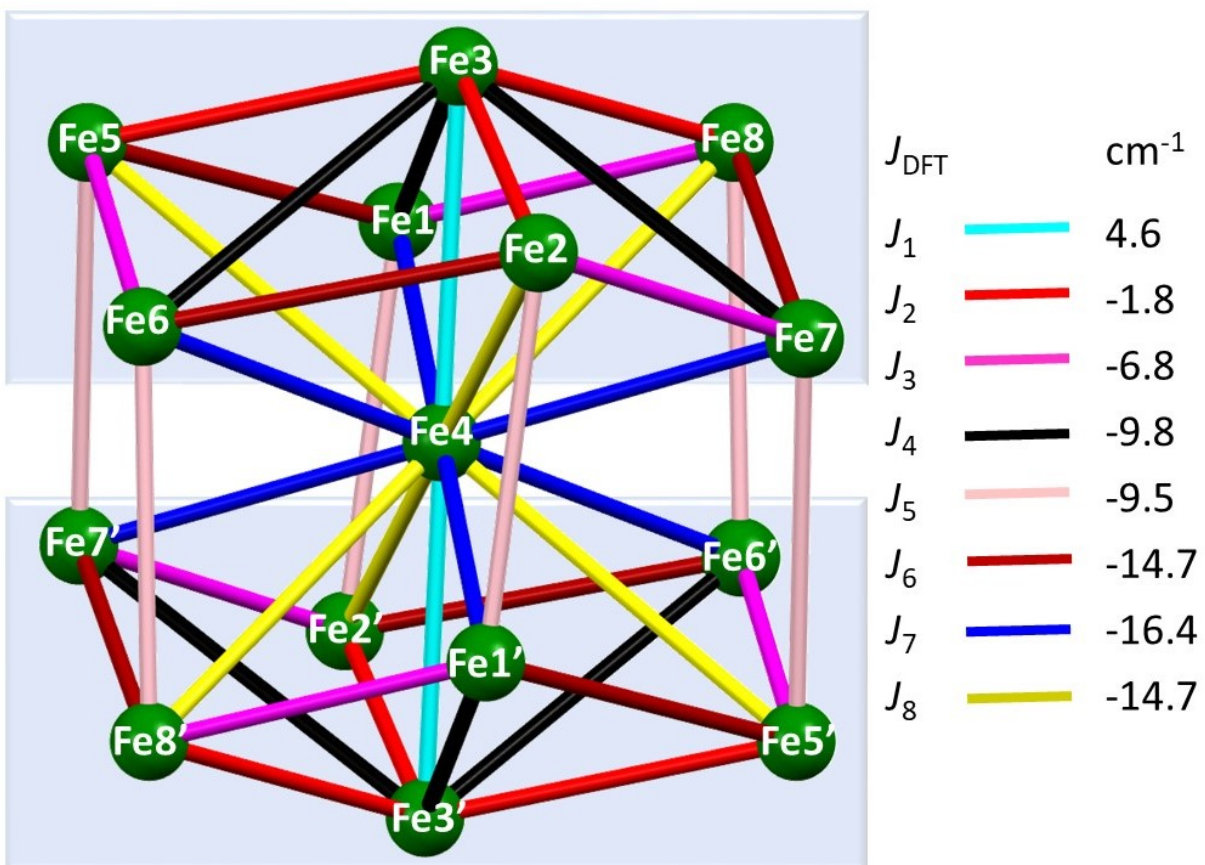
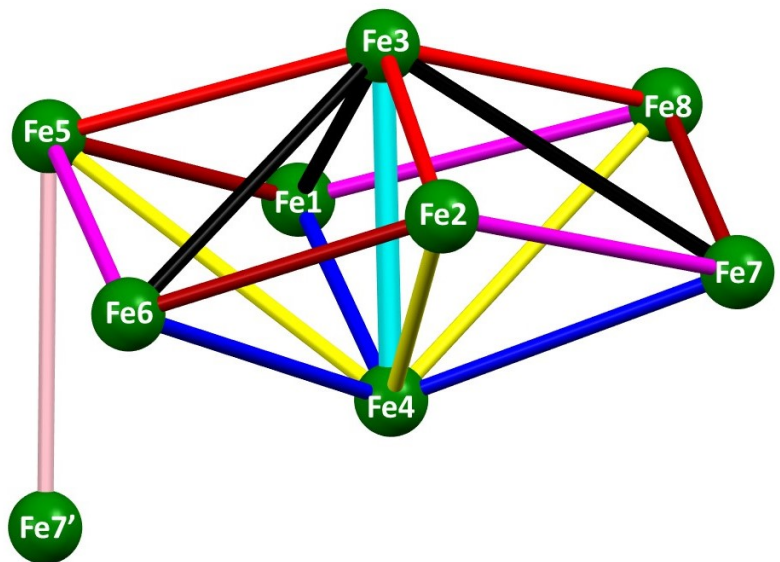


Figure S11: Schematic representation of the eight independent magnetic exchange interactions in model **1A** (top) and complex **1** (bottom).

Table S3. DFT computed magnetic exchange interactions calculated for model complex **1A**, together with pertinent structural parameters for **1**. N = total number of individual interactions present. $\sum |S_{AB}|$ represents the total overlap integrals (OIs).

N J_{DFT}	Bridging group(s)	J / cm^{-1}	Avg. Fe-O distance	Avg. Fe-O-Fe angle ($^{\circ}$)	Fe-Fe distance	$\sum S_{AB}$
$2 \times J_1$	$3\mu_4\text{-O}^{2-}$	+4.6	2.245	86.7	3.102	0.433
$6 \times J_2$	$\mu_2\text{-O-CH}_2\text{-CH}_2\text{-N(R)}$,	-1.8	2.103	102.1	3.246	0.570
$6 \times J_3$	$\mu_2\text{-O-CH}_2\text{-CH}_2\text{-N(R)}$,	-6.8	1.985	99.1	3.022	0.761
$6 \times J_4$	$\mu_4\text{-O}^{2-}$	-9.8	2.208	111.1	3.657	0.800
$6 \times J_5$	$\mu_2\text{-O-CH}_2\text{-CH}_2\text{-N(R)}$	-9.5	1.991	116.7	3.390	0.799
$6 \times J_6$	$\mu_2\text{-O-CH}_2\text{-CH}_2\text{-N(R)}$	-14.7	1.935	129.4	3.500	1.054
$6 \times J_7$	$\mu_4\text{-O}^{2-}$	-16.4	1.963	117.4	3.354	1.221
$6 \times J_8$	$\mu_4\text{-O}^{2-}$	-14.7	2.012	140.8	3.791	1.063

Table S4. DFT computed overlap integral (OI) values for $J_1\text{-}J_8$. Here α and β signify spin-up and spin-down orbitals, respectively. $\sum |S_{AB}|$ represents the total OIs between Fe^{III}-Fe^{III} SOMOs. Red and blue numbers represent strong and intermediate interactions, respectively.

$J_1 = 4.6 \text{ cm}^{-1} (\alpha/\beta)$	$3d_{yz}$	$3d_{xz}$	$3d_z^2$	$3d_{xy}$	$3d_{x^2-y^2}$	$\sum S_{AB} $
$3d_{yz}$	0.028	0.013	0.033	0.013	0.017	0.433
$3d_{xy}$	0.043	0.005	0.035	0.041	0.019	
$3d_{xz}$	0.000	0.001	0.104	0.012	0.004	
$3d_z^2$	0.004	0.012	0.001	0.002	0.008	
$3d_{x^2-y^2}$	0.011	0.006	0.006	0.004	0.011	

$J_2 = -1.8 \text{ cm}^{-1} (\alpha/\beta)$	$3d_{yz}$	$3d_{xz}$	$3d_z^2$	$3d_{xy}$	$3d_{x^2-y^2}$	$\sum S_{AB} $
$3d_{yz}$	0.054	0.007	0.010	0.054	0.004	0.570
$3d_{xy}$	0.003	0.003	0.025	0.017	0.020	
$3d_{xz}$	0.068	0.005	0.009	0.009	0.009	
$3d_{x^2-y^2}$	0.005	0.001	0.006	0.029	0.010	
$3d_z^2$	0.046	0.039	0.018	0.060	0.059	

$J_3 = -6.8 \text{ cm}^{-1} (\alpha/\beta)$	$3d_{yz}$	$3d_{xy}$	$3d_{xz}$	$3d_{x^2-y^2}$	$3d_z^2$	$\sum S_{AB} $
$3d_{yz}$	0.071	0.006	0.037	0.002	0.033	0.761
$3d_{xy}$	0.000	0.004	0.004	0.023	0.095	
$3d_z^2$	0.019	0.032	0.050	0.011	0.022	
$3d_{xz}$	0.029	0.003	0.044	0.162	0.014	
$3d_{x^2-y^2}$	0.012	0.041	0.005	0.024	0.018	

$J_4 = -9.8 \text{ cm}^{-1} (\alpha/\beta)$	$3d_{yz}$	$3d_{xz}$	$3d_z^2$	$3d_{xy}$	$3d_{x^2-y^2}$	$\sum S_{AB} $
$3d_{yz}$	0.040	0.004	0.074	0.011	0.016	0.800
$3d_{xy}$	0.104	0.043	0.026	0.020	0.005	
$3d_{xz}$	0.091	0.029	0.033	0.003	0.005	
$3d_z^2$	0.092	0.041	0.027	0.024	0.012	
$3d_{x^2-y^2}$	0.018	0.003	0.016	0.027	0.036	

$J_5 = -9.5 \text{ cm}^{-1} (\alpha/\beta)$	$3d_{yz}$	$3d_{xy}$	$3d_{xz}$	$3d_{x^2-y^2}$	$3d_z^2$	$\sum S_{AB} $
$3d_{yz}$	0.033	0.006	0.027	0.004	0.078	0.799

$3d_{xy}$	0.010	0.010	0.014	0.027	0.020	
$3d_{xz}$	0.020	0.026	0.015	0.015	0.054	
$3d_z^2$	0.045	0.010	0.028	0.097	0.040	
$3d_x^2-y^2$	0.012	0.062	0.004	0.117	0.025	
$J_6 = -14.7 \text{ cm}^{-1} (\alpha/\beta)$	$3d_{yz}$	$3d_{xy}$	$3d_{xz}$	$3d_x^2-y^2$	$3d_z^2$	$\sum S_{AB} $
$3d_{yz}$	0.050	0.088	0.073	0.011	0.014	1.054
$3d_{xy}$	0.013	0.013	0.029	0.088	0.084	
$3d_{xz}$	0.001	0.034	0.009	0.000	0.041	
$3d_z^2$	0.010	0.012	0.006	0.109	0.007	
$3d_x^2-y^2$	0.011	0.047	0.002	0.226	0.076	
$J_7 = -16.4 \text{ cm}^{-1} (\alpha/\beta)$	$3d_{xy}$	$3d_{yz}$	$3d_{xz}$	$3d_z^2$	$3d_x^2-y^2$	$\sum S_{AB} $
$3d_{yz}$	0.029	0.105	0.047	0.009	0.103	1.221
$3d_{xy}$	0.02	0.068	0.012	0.072	0.066	
$3d_{xz}$	0.006	0.009	0.018	0.025	0.005	
$3d_z^2$	0.005	0.038	0.037	0.129	0.092	
$3d_x^2-y^2$	0.095	0.052	0.025	0.139	0.015	
$J_8 = -14.7 \text{ cm}^{-1} (\alpha/\beta)$	$3d_{yz}$	$3d_{xy}$	$3d_{xz}$	$3d_z^2$	$3d_x^2-y^2$	$\sum S_{AB} $
$3d_{yz}$	0.007	0.011	0.013	0.006	0.001	1.063
$3d_{xy}$	0.010	0.204	0.166	0.097	0.020	
$3d_{xz}$	0.026	0.002	0.006	0.037	0.019	
$3d_x^2-y^2$	0.008	0.044	0.049	0.091	0.066	
$3d_z^2$	0.027	0.038	0.007	0.055	0.053	

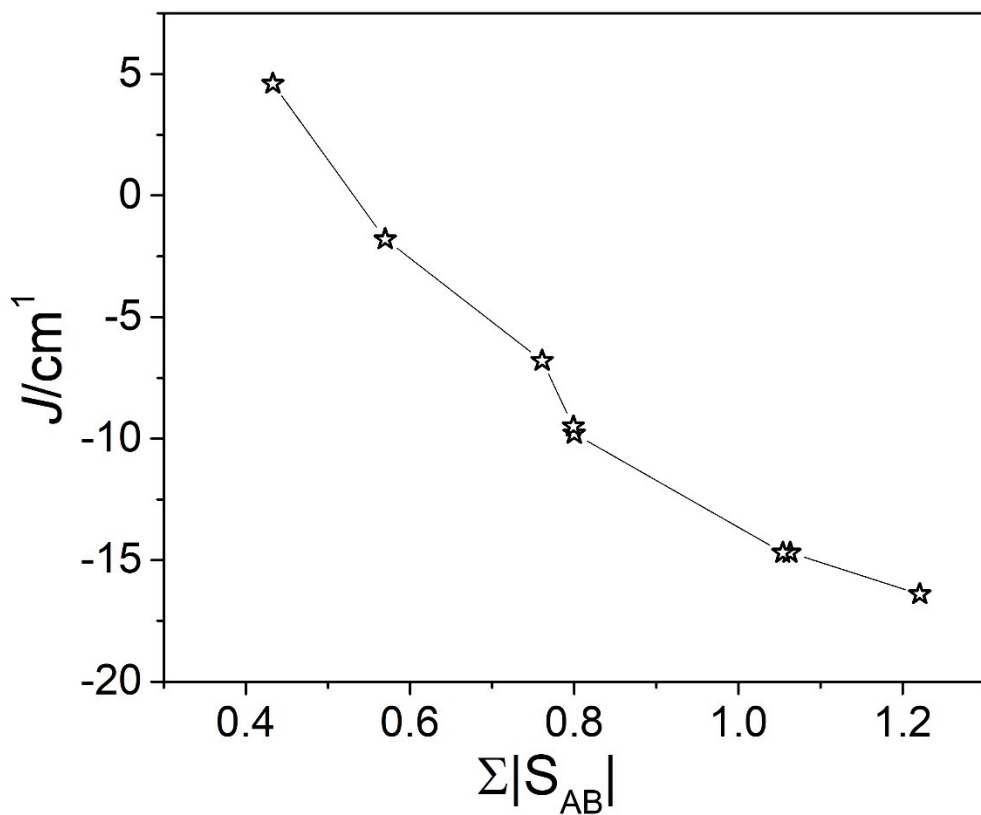
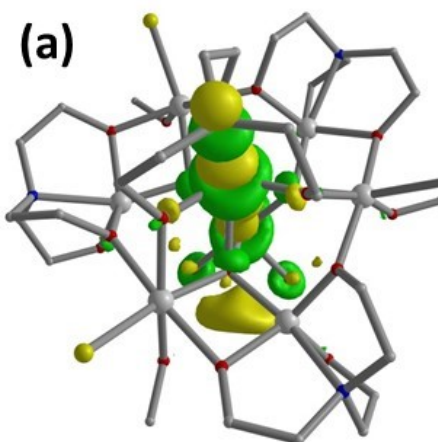
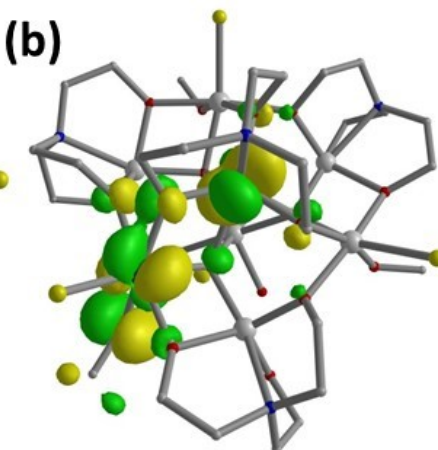


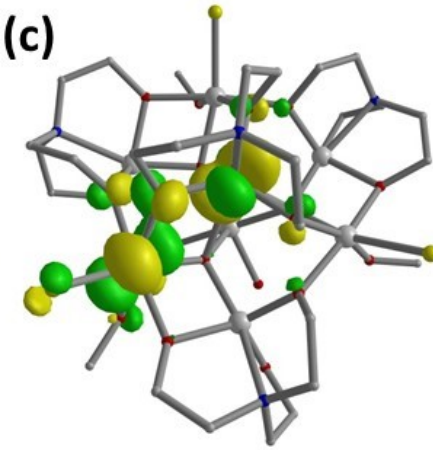
Figure S12. Plot of DFT estimated magnetic exchange interactions (J_1-J_8) with respect to their total overlap integral value ($\sum|S_{AB}|$). In general, larger the total overlap integral, the stronger the antiferromagnetic exchange interaction, and vice versa.⁶



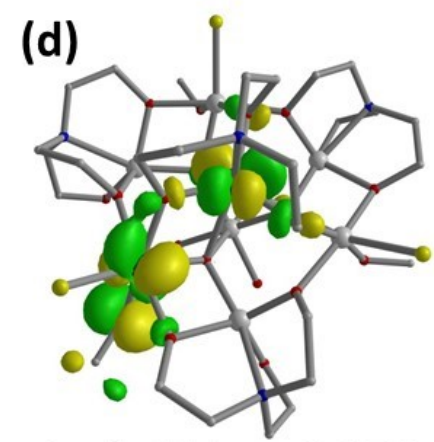
$$J_1; d_z^2 \parallel d_{xz} = 0.104$$



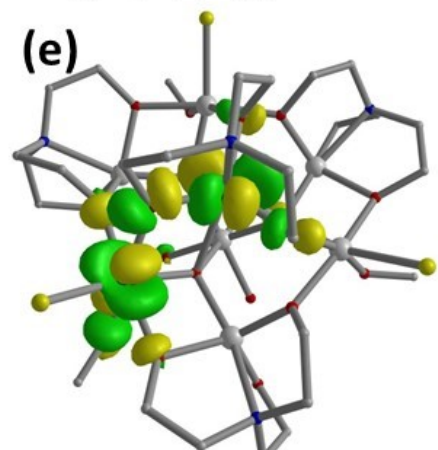
$$J_2; d_{yz} \parallel d_{yz} = 0.054$$



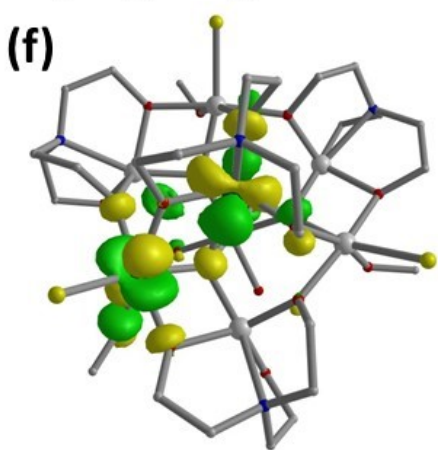
$$J_2; d_{yz} \parallel d_{xz} = 0.068$$



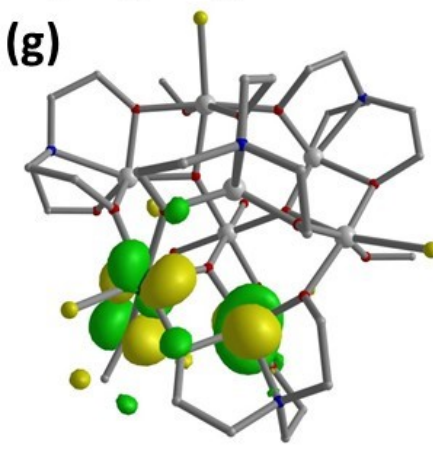
$$J_2; d_{xy} \parallel d_{yz} = 0.054$$



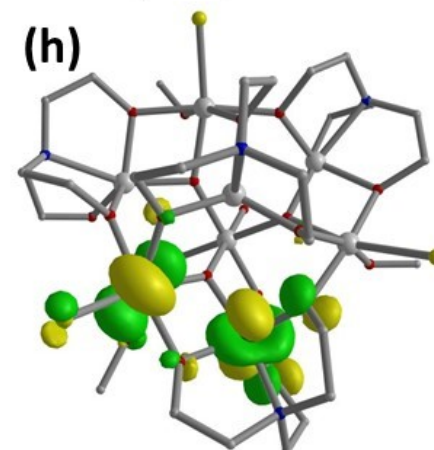
$$J_2; d_{xy} \parallel d_{z^2} = 0.060$$



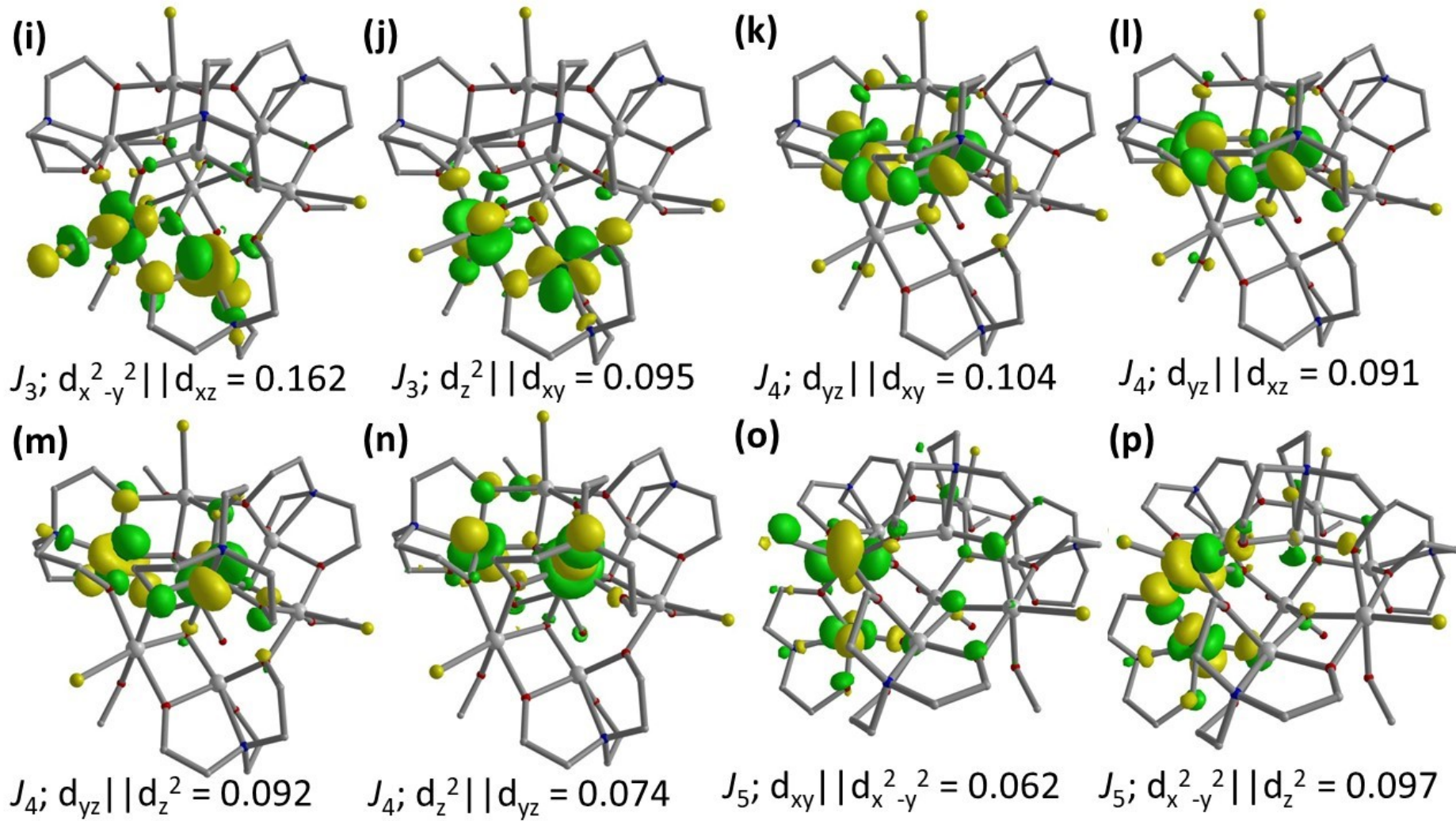
$$J_2; d_{x^2-y^2} \parallel d_{z^2} = 0.059$$

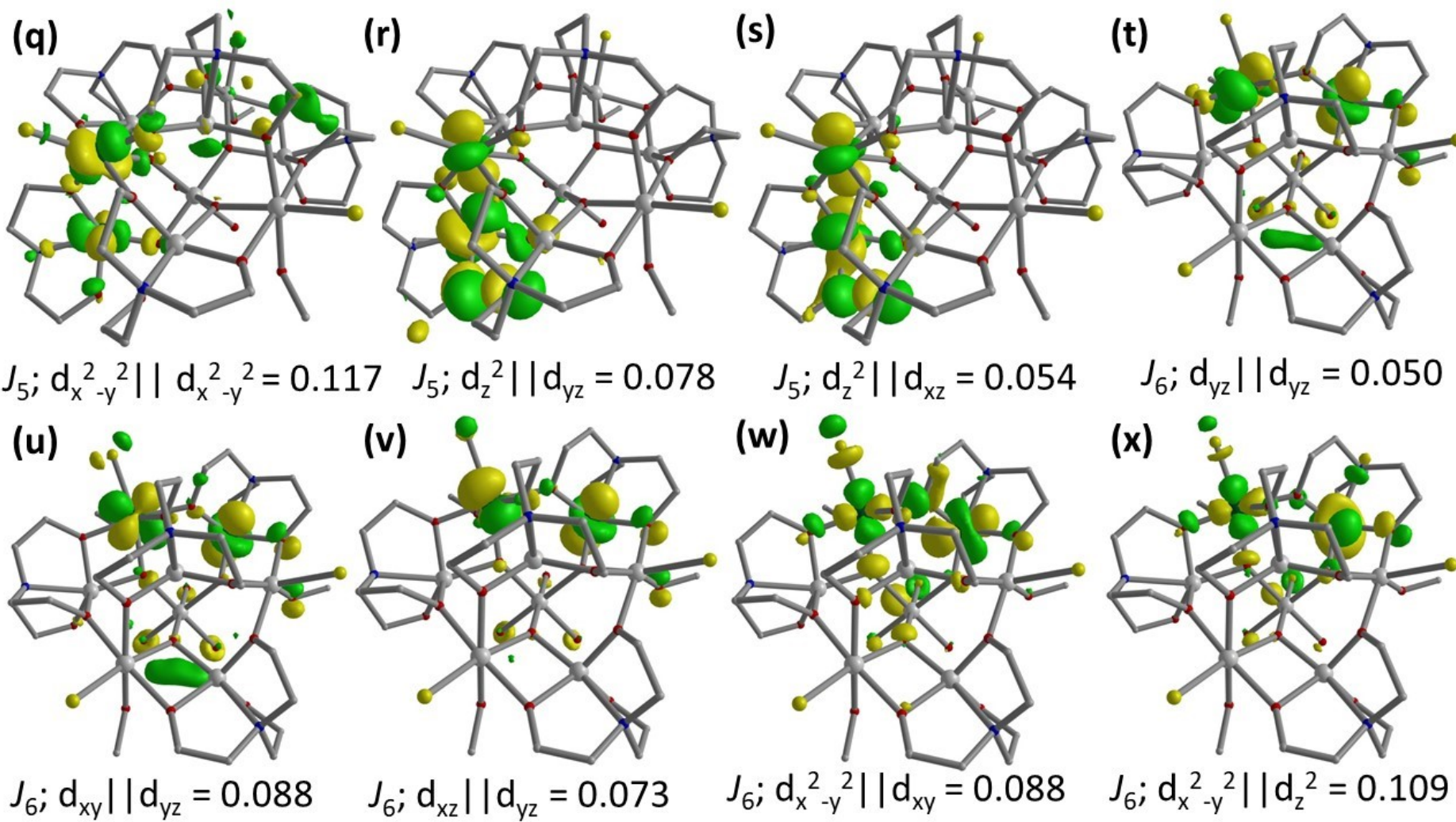


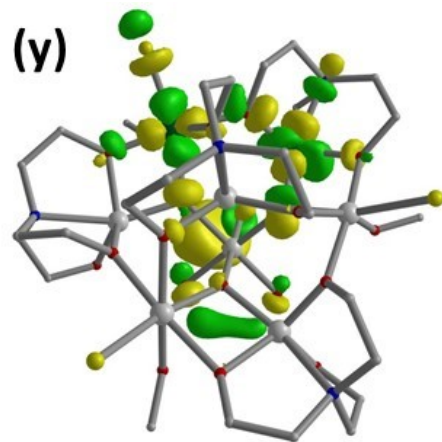
$$J_3; d_{yz} \parallel d_{yz} = 0.071$$



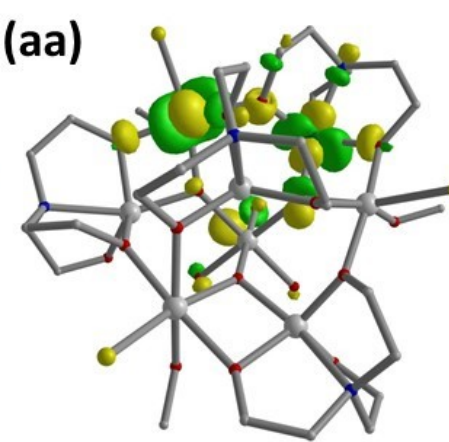
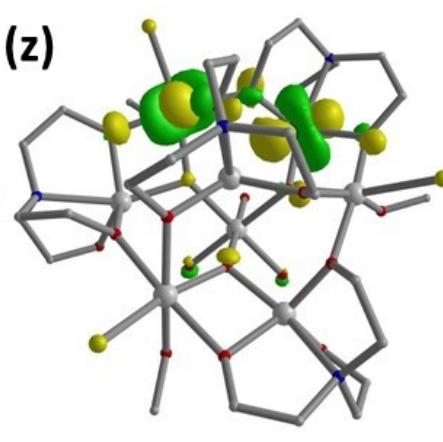
$$J_3; d_{xz} \parallel d_{z^2} = 0.050$$



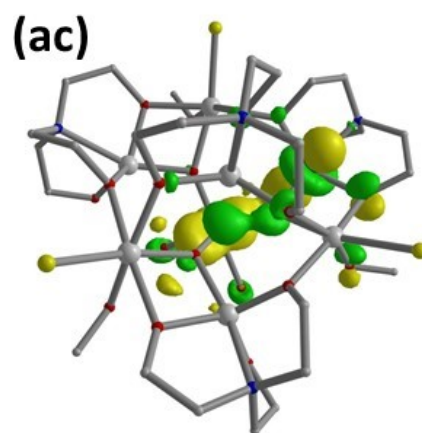
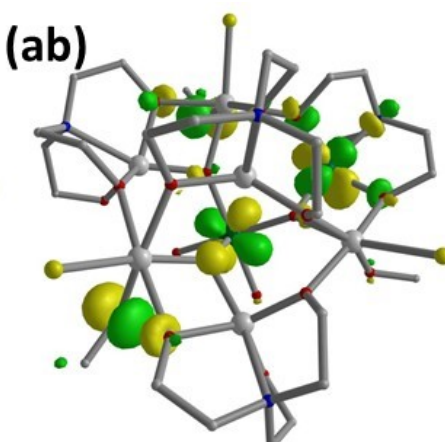




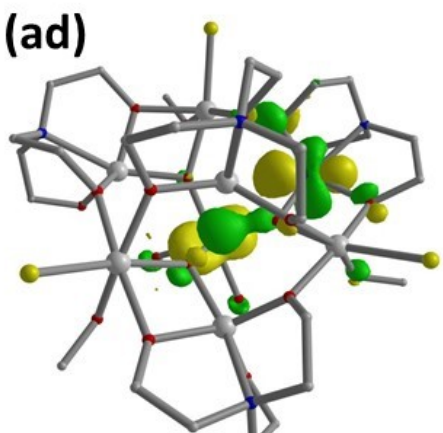
$$J_6; d_{x^2-y^2}^2 || d_{x^2-y^2}^2 = 0.226 \quad J_6; d_z^2 || d_{xy} = 0.084$$



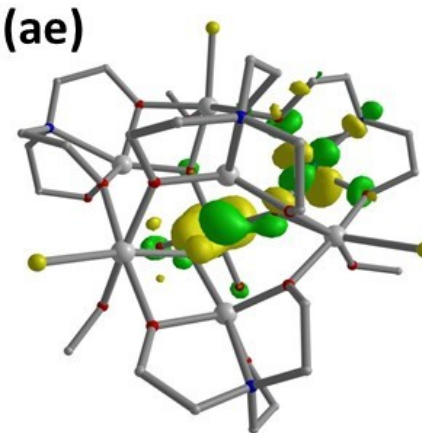
$$J_6; d_z^2 || d_{x^2-y^2}^2 = 0.076 \quad J_7; d_{xy} || d_{x^2-y^2}^2 = 0.095$$



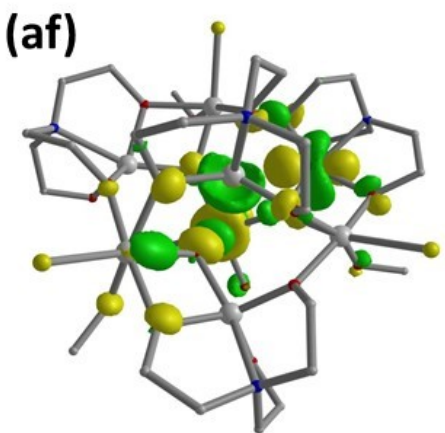
$$J_7; d_{yz} || d_{yz} = 0.105$$



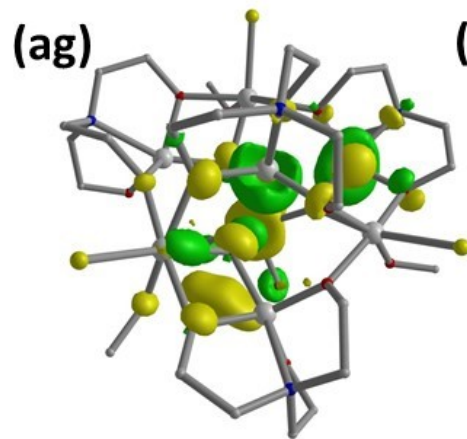
$$J_7; d_{yz} || d_{xy} = 0.068$$



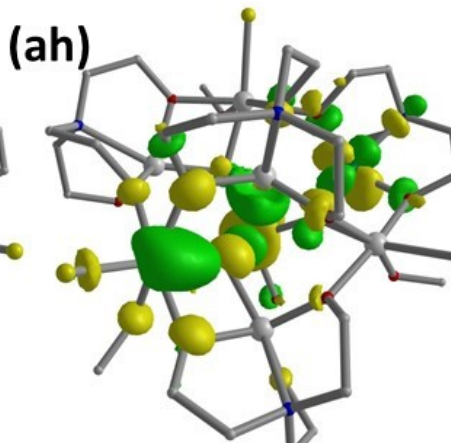
$$J_7; d_{yz} || d_{x^2-y^2}^2 = 0.052$$



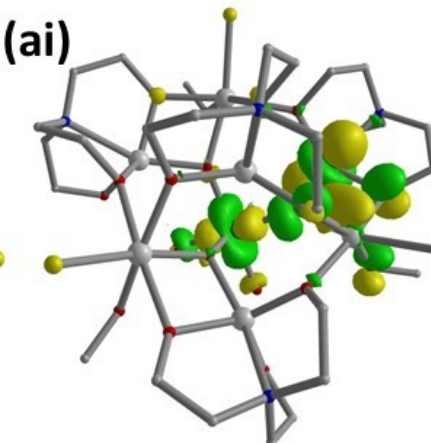
$$J_7; d_z^2 || d_{xy} = 0.072$$



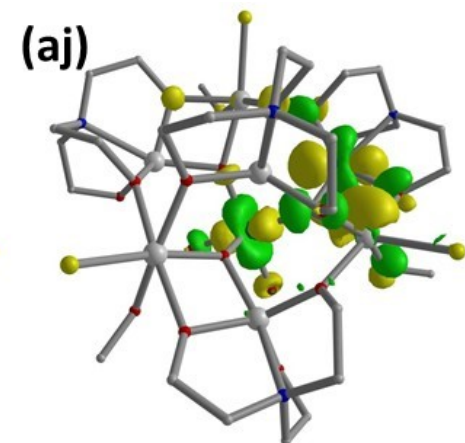
$$J_7; d_z^2 \parallel d_z^2 = 0.129$$



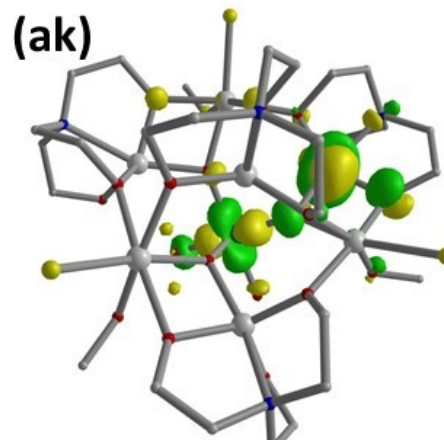
$$J_7; d_z^2 \parallel d_{x^2-y^2}^2 = 0.139$$



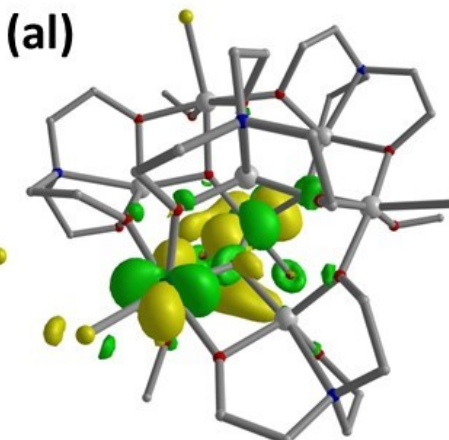
$$J_7; d_{x^2-y^2}^2 \parallel d_{yz} = 0.103$$



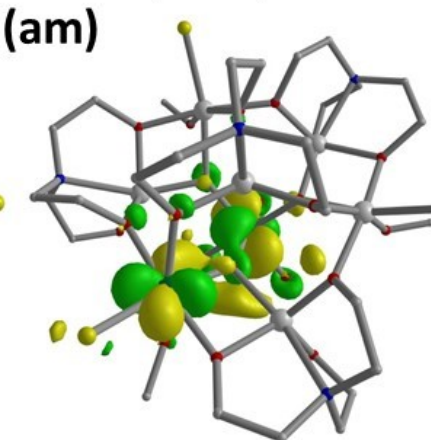
$$J_7; d_{x^2-y^2}^2 \parallel d_{xy} = 0.066$$



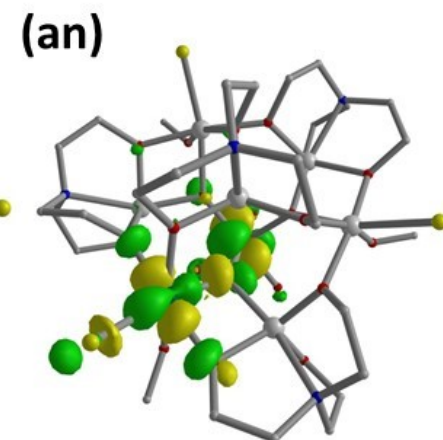
$$J_7; d_{x^2-y^2}^2 \parallel d_z^2 = 0.092$$



$$J_8; d_{xy} \parallel d_{xy} = 0.204$$



$$J_8; d_{xz} \parallel d_{xy} = 0.166$$



$$J_8; d_{xz} \parallel d_{x^2-y^2}^2 = 0.049$$

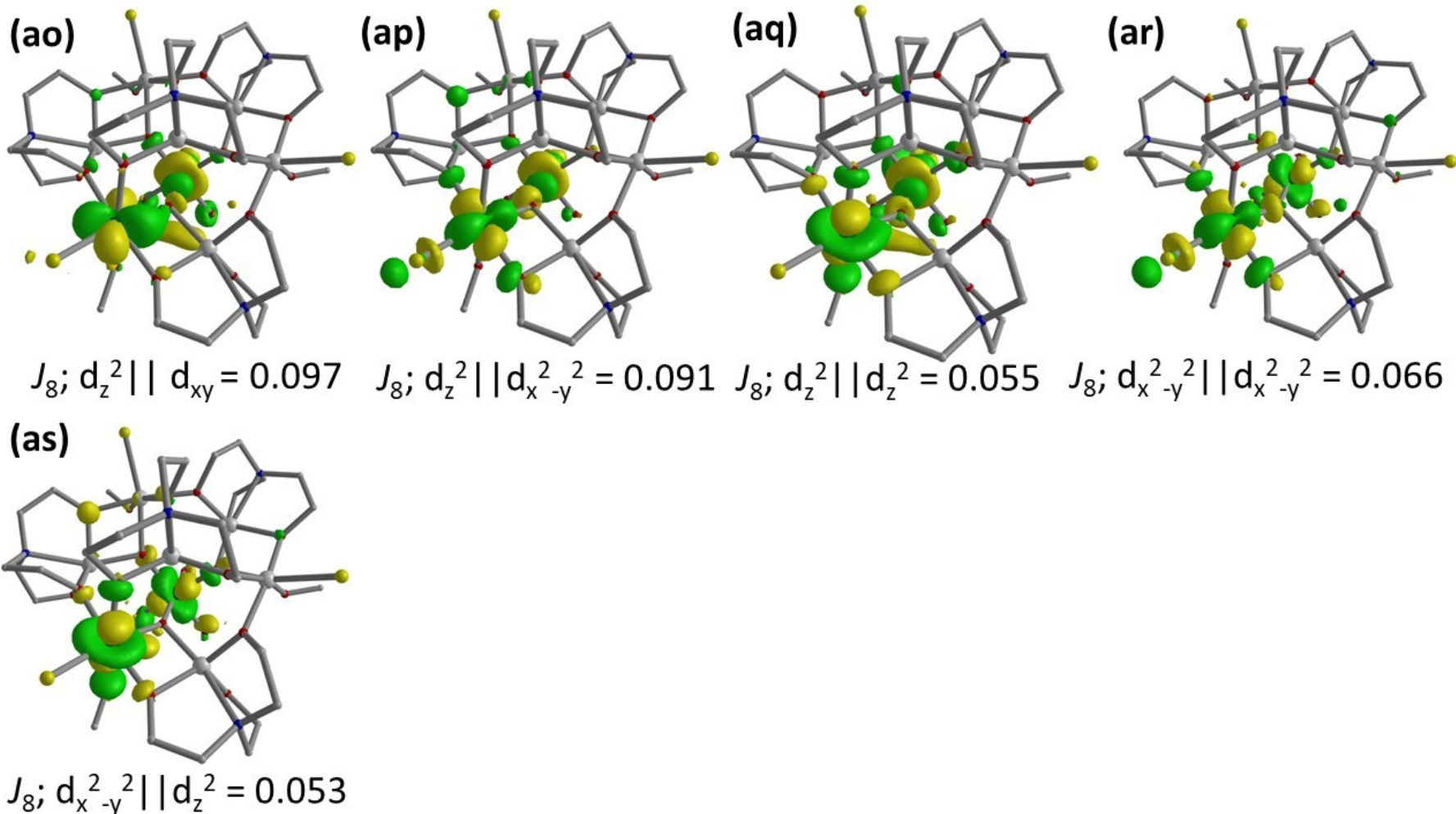


Figure S13. DFT calculated strong and intermediate overlap integrals corresponding to (a) J_1 ; (b-f) J_2 ; (g-j) J_3 ; (k-n) J_4 ; (o-s) J_5 ; (t-aa) J_6 ; (ab-ak) J_7 and (al-as) J_8 .

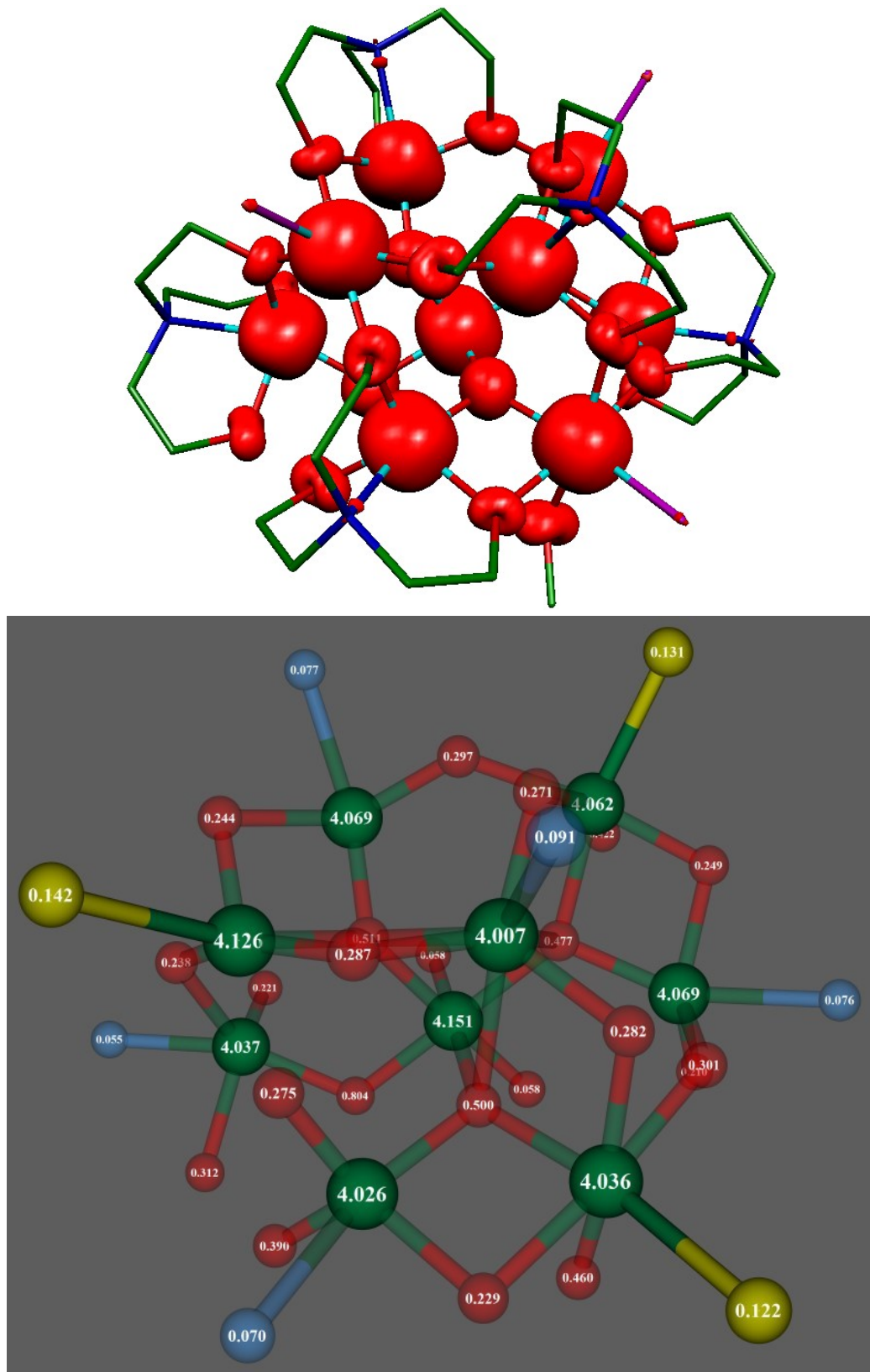


Figure S14. DFT computed spin density plot (top) together with the spin density values on the important atoms for model **1A** (bottom). Strong spin delocalization is observed for model **1A** with spin densities on the Fe^{III} ions ranging between 4.007-4.151.

References

1. G. M. Sheldrick, *Acta Crystallogr. Sect. C: Cryst. Struct. Commun.*, 2015, **71**, 3-8.
2. O. V. Dolomanov, L. J. Bourhis, R. J. Gildea, J. A. K. Howard and H. Puschmann, *J. Appl. Crystallogr.*, 2009, **42**, 339-341.
3. M. J. Frisch, G. W. Trucks, H. B. Schlegel, G. E. Scuseria, M. A. Robb, J. R. Cheeseman, G. Scalmani, V. Barone, G. A. Petersson, H. Nakatsuji, X. Li, M. Caricato, A. V. Marenich, J. Bloino, B. G. Janesko, R. Gomperts, B. Mennucci, H. P. Hratchian, J. V. Ortiz, A. F. Izmaylov, J. L. Sonnenberg, Williams, F. Ding, F. Lipparini, F. Egidi, J. Goings, B. Peng, A. Petrone, T. Henderson, D. Ranasinghe, V. G. Zakrzewski, J. Gao, N. Rega, G. Zheng, W. Liang, M. Hada, M. Ehara, K. Toyota, R. Fukuda, J. Hasegawa, M. Ishida, T. Nakajima, Y. Honda, O. Kitao, H. Nakai, T. Vreven, K. Throssell, J. A. Montgomery Jr., J. E. Peralta, F. Ogliaro, M. J. Bearpark, J. J. Heyd, E. N. Brothers, K. N. Kudin, V. N. Staroverov, T. A. Keith, R. Kobayashi, J. Normand, K. Raghavachari, A. P. Rendell, J. C. Burant, S. S. Iyengar, J. Tomasi, M. Cossi, J. M. Millam, M. Klene, C. Adamo, R. Cammi, J. W. Ochterski, R. L. Martin, K. Morokuma, O. Farkas, J. B. Foresman and D. J. Fox, Gaussian, Inc., Wallingford CT, 2016.
4. M. Coletta, S. Sanz, D. J. Cutler, S. J. Teat, K. J. Gagnon, M. K. Singh, E. K. Brechin and S. J. Dalgarno, *Dalton Trans.*, 2020, **49**, 14790-14797.
5. A. E. Dearle, D. J. Cutler, H. W. L. Fraser, S. Sanz, E. Lee, S. Dey, I. F. Diaz-Ortega, G. S. Nichol, H. Nojiri, M. Evangelisti, G. Rajaraman, J. Schnack, L. Cronin and E. K. Brechin, *Angew. Chem. Int. Ed.*, 2019, **58**, 16903-16906.
6. M. Coletta, T. G. Tziotzi, M. Gray, G. S. Nichol, M. K. Singh, C. J. Milius and E. K. Brechin, *Chem. Commun.*, 2021, **57**, 4122-4125.
7. L. Noodleman, *J. Chem. Phys.*, 1981, **74**, 5737.
8. A. D. Becke, *Phys. Rev. A*, 1988, **38**, 3098-3101.
9. A. D. Becke, *J. Chem. Phys.*, 1993, **98**, 5648.
10. C. Lee, W. Yang and R. G. Parr, *Phys. Rev. B: Condens. Matter Mater. Phys.*, 1988, **37**, 785.
11. A. Schäfer, H. Horn and R. Ahlrichs, *J. Chem. Phys.*, 1992, **97**, 2571-2577.
12. A. Schäfer, C. Huber and R. Ahlrichs, *J. Chem. Phys.*, 1994, **100**, 5829.
13. G. E. Scuseria and H. F. Schäfer, *J. Chem. Phys.*, 1989, **90**, 3700.
14. V. A. Rassolov, J. A. Pople, M. A. Ratner and T. L. Windus, *J. Chem. Phys.*, 1998, **109**, 1223-1229.
15. M. K. Singh, *Dalton Trans.*, 2020, **49**, 4539-4548.
16. M. K. Singh and G. Rajaraman, *Inorg. Chem.*, 2019, **58**, 3175-3188.
17. M. K. Singh and G. Rajaraman, *Chem. Eur. J.*, 2015, **21**, 980-983.
18. J. Caballero-Jiménez, F. Habib, D. Ramírez-Rosales, R. Grande-Aztatzi, G. Merino, I. Korobkov, M. K. Singh, G. Rajaraman, Y. Reyes-Ortega and M. Murugesu, *Dalton Trans.*, 2015, **44**, 8649.
19. C. McDonald, S. Sanz, E. K. Brechin, M. K. Singh, G. Rajaraman, D. Gaynor and L. F. Jones, *RSC Adv.*, 2014, **4**, 38182.
20. G. Rajaraman, E. Ruiz, J. Cano and S. Alvarez, *Chem. Phys. Lett.*, 2005, **415**, 6.

21. T. Cauchy, E. Ruiz and S. Alvarez, *J. Am. Chem. Soc.*, 2006, **128**, 15722-15727.
22. T. Cauchy, E. Ruiz and S. Alvarez, *Phys. B*, 2006, **384**, 116.
23. E. Ruiz, J. Cano and S. Alvarez, *Chem. Eur. J.*, 2005, **11**, 4767.
24. R. Carrasco, J. Cano, T. Mallah, L. F. Jones, D. Collison and E. K. Brechin, *Inorg. Chem.*, 2004, **43**, 5410-5415.